Fermilab FERMILAB-Pub-02/027-A February 2002

Loose Groups of Galaxies in the Las Campanas Redshift Survey

Douglas L. Tucker
Fermi National Accelerator Laboratory, MS 127, P.O. Box 500, Batavia, IL 60510, USA;
dtucker@fnal.gov

Augustus Oemler, Jr.[1], Yasuhiro Hashimoto[1,2], and Stephen A. Shectman
Carnegie Observatories, 813 Santa Barbara Street, Pasadena, CA 91101, USA;
oemler@ociw.edu, hashimoto@vorpal.ociw.edu, shec@ociw.edu

Robert P. Kirshner
Harvard-Smithsonian Center for Astrophysics, 60 Garden Street, Cambridge, MA 02138,
USA; kirshner@cfa.harvard.edu

Huan Lin[3]
Steward Observatory, University of Arizona, 933 N. Cherry Ave., Tucson, AZ 85721, USA;
hlin@as.arizona.edu

Stephen D. Landy
Dept. of Physics, College of William & Mary, Williamsburg, VA 23187, USA;
landy@physics.wm.edu

Paul L. Schechter
Dept. of Physics, Massachusetts Institute of Technology, Cambridge, MA 02139, USA;
schech@achernar.mit.edu

and

Sahar S. Allam[4]
National Research Institute for Astronomy & Geophysics, Helwan Observatory, Cairo,
Egypt; shr@frcu.eun.eg

ABSTRACT

[1]Also: Dept. of Astronomy, Yale University, New Haven, CT 06520-8101, USA.

[2]Present Address: Astrophysikalisches Institut Potsdam, An der Sternwarte 16, D-14482 Potsdam, Germany.

[3]Hubble Fellow.

[4]Visiting Scientist, Fermi National Accelerator Laboratory.

A “friends-of-friends” percolation algorithm has been used to extract a catalogue of $\delta n/n = 80$ density enhancements (groups) from the six slices of the Las Campanas Redshift Survey (LCRS). The full catalogue contains 1495 groups and includes 35% of the LCRS galaxy sample. A clean sample of 394 groups has been derived by culling groups from the full sample which either are too close to a slice edge, have a crossing time greater than a Hubble time, have a corrected velocity dispersion of zero, or contain a 55-arcsec “orphan” (a galaxy with a mock redshift which was excluded from the original LCRS redshift catalogue due to its proximity to another galaxy — i.e., within 55 arcsec). Median properties derived from the clean sample include: line-of-sight velocity dispersion $\sigma_{\rm los} = 164$ km s^{-1}, crossing time $t_{\rm cr} = 0.10\ H_0^{-1}$, harmonic radius $R_{\rm h} = 0.58\ h^{-1}$ Mpc, pairwise separation $R_{\rm p} = 0.64\ h^{-1}$ Mpc, virial mass $M_{\rm vir} = 1.90 \times 10^{13}\ h^{-1}\ M_{\odot}$, total group R-band luminosity $L_{\rm tot} = 1.30 \times 10^{11}\ h^{-2}\ L_{\odot}$, and R-band mass-to-light ratio $M/L = 171\ h\ M_{\odot}/L_{\odot}$; the median number of observed members in a group is 3.

Subject headings: catalogs — cosmology: large-scale structure of the universe — galaxies: clusters: general — galaxies: distances and redshifts — surveys

1. Introduction to Group Catalogues

Loose groups of galaxies are important but little-understood entities. They are intermediate in scale between galaxies and rich clusters, and thus their dynamics are important in the study of the distribution of dark matter on scales greater than haloes of galaxies but smaller than the typical sizes of large clusters [see, for example, the review by Oemler (1988)]. Their environment is also intermediate between that of isolated galaxies and that of the cores of rich clusters, and therefore the study of groups may provide clues to the processes that create the observed dependency of galaxy morphology on environment (Postman & Geller 1984; Oemler 1992; Allington-Smith et al. 1993; Whitmore, Gilmore, & Jones 1993; Zabludoff et al. 1996; Hashimoto et al. 1998). Only in the past 15 years, however, with the advent of extensive galaxy redshift surveys, have suitably uncontaminated, objective group catalogues been available for study.

Galaxies and rich clusters of galaxies are generally easy to identify. They are high-contrast objects compared with their immediate surroundings. Unfortunately, loose groups of galaxies, which are neither particularly dense nor exceptionally populous, are much more difficult to distinguish from their surroundings. Early group catalogues were based upon the identification of galaxy concentrations on the sky, first primarily by visual inspection of photographic plates (e.g., Holmberg 1969, de Vaucouleurs 1975), and, later, via objective group-finding algorithms (e.g., Turner & Gott 1976). Since these group catalogues relied especially on just the two dimensions of spatial information available on the plane of the sky, they were greatly subject to contamination from projection effects. Projection effects are largely mitigated (although never fully eliminated) in group catalogues derived from galaxy redshift surveys. In the early-1980's, Huchra & Geller (1982; HG82), pioneers in the extraction of groups from redshift surveys by means of objective, "friends-of-friends" percolation algorithms, compiled a group catalogue from a shallow ($m_{B(0)}^{\rm lim} = 13.2$) whole-sky redshift catalogue containing 1312 galaxies. They later derived a group catalogue from the original ($m_{B(0)}^{\rm lim} = 14.5$) CfA Survey (hereafter, CfA1) (Geller & Huchra 1983; GH83). The CfA1 has in fact proved to be a popular testing ground for group-finding algorithms; additional group catalogues drawn from the CfA1 include those by Nolthenius & White (1987; NW87), Nolthenius (1993; N93), and Moore, Frenk, & White (1993; MFW93). Groups have also been identified in a 12° slice from the CfA extension to $m_{B(0)}^{\rm lim} = 15.5$ [henceforth, CfA2; Ramella, Geller, & Huchra 1989 (RGH89)] and in the diameter-limited Southern Sky Redshift Survey [SSRS; Maia, da Costa, & Latham 1989 (MdCL89)]. More recently, group catalogues have been extracted from the full northern CfA2 by Ramella, Pisani, & Geller (1997; RPG97), from the Pisces-Perseus redshift survey (PPS) by Trasarti-Battistoni (1998; TB98), and from the ESO Slice Project (ESP) galaxy redshift survey by Ramella et al. (1999; RZZ99).

In this paper, we will present a group catalogue based upon the Las Campanas Redshift Survey (LCRS; Shectman et al. 1996). Due to the large volume this survey samples, the LCRS includes numerous "Great Wall"-like structures within its borders and is therefore one of the first redshift surveys which can claim to enclose a reasonably fair sample of the nearby Universe. With the exception of the ESP, the redshift surveys from which the aforementioned group catalogues have been derived have all tended to be dominated by a very few large structures. Therefore, a group catalogue based upon the LCRS should be found to contain groups in a wider range of environments than the groups identified from these shallower surveys. A census of group properties based upon LCRS groups would thus be more complete, and therefore more useful for studies of both galaxy dynamics and environmental dependences. In fact, this characteristic is so important that earlier variations of the present catalogue have already been used in studies of the environmental influence on galaxy morphology (Hashimoto & Oemler 1998), on the presence of "E+A" galaxies (Zabludoff et al. 1996), and on the general rate of star formation within galaxies (Hashimoto et al. 1998, Allam et al. 1999).

We divide the remainder of this paper as follows: we describe the LCRS galaxy sample in § 2, discuss the modified "friends-of-friends" algorithm used to extract the LCRS group catalogue in § 3, present the catalogue itself in § 4, and compare it with various group catalogues and with Abell clusters [Abell 1958; Abell, Corwin, & Olowin 1989 (ACO)] in § 5 and § 6; in § 7, we summarize and conclude.

2. The Data

The LCRS is an optically selected galaxy redshift survey which extends to a redshift of 0.2 and which is composed of a total of 6 alternating $1.5^{\circ} \times 80^{\circ}$ slices, 3 each in the North and South Galactic Caps. Completed in 1996, the LCRS contains 26,418 galaxy redshifts, of which 23,697 lie within the official geometric and photometric limits of the survey. Accurate R-band photometry and sky positions for program objects were extracted from CCD drift scans obtained on the Las Campanas Swope 1-m telescope; spectroscopy was performed at the Las Campanas Du Pont 2.5-m telescope, originally via a 50-fiber Multi-Object Spectrograph (MOS), and later via a 112-fiber MOS. For observing efficiency, all the fibers were used, but each MOS field was observed only once. Hence, the LCRS is a collection of 50-fiber fields (with nominal apparent magnitude limits of $16.0 \leq R < 17.3$) and 112-fiber fields (with nominal apparent magnitude limits of $15.0 \leq R < 17.7$); see Figure 1. Thus, selection criteria vary from field to field, but these selection criteria are carefully documented and therefore easily taken into account. Observing each field only once, however, creates an additional selection effect: the protective tubing of the individual fibers prevents the spectroscopic observation of both members of galaxy pairs within 55 arcsec of each other. Hence, groups and clusters can be undersampled, potentially causing physical groups to be split by a "friends-of-friends" percolation algorithm and resulting in the mis-estimate of general group properties. We will return to this problem in the next section.

In constructing the group catalogue, we have considered only those LCRS galaxies within the official geometric and photometric borders of the survey; we have furthermore limited this sample to galaxies having redshifts in the range

$$7,500 \text{ km s}^{-1} \leq cz < 50,000 \text{ km s}^{-1} \tag{1}$$

and luminosities in the range

$$-22.5 \leq M_R - 5\log h < -17.5. \tag{2}$$

To avoid group-member incompleteness at the extremal distances of the sample, only groups within

$$10,000 \text{ km s}^{-1} \leq cz < 45,000 \text{ km s}^{-1} \tag{3}$$

were admitted into the final group catalogue.

[N.B.: Unless otherwise noted, all redshifts z in this text are corrected for motion relative to the dipole moment of the cosmic microwave background (CMB; Lineweaver et al. 1996).]

3. Extracting the Group Catalogue

3.1. The "Friends-of-Friends" Algorithm

The LCRS group catalogue was extracted by means of an adaptive "friends-of-friends" percolation algorithm based upon that of HG82 and modified for use with comoving distances and field-to-field sampling variations.

We outline the procedure as follows: First, a seed galaxy ("galaxy i") is selected which has not yet been classified as either a group member or an isolated galaxy. Every other non-classified galaxy j in the survey sample is then tested to see if it lies within a projected separation $D_{\rm L}$ and a velocity difference $V_{\rm L}$ of the seed galaxy (note that both $D_{\rm L}$ and $V_{\rm L}$ are functions of both the field f and of the mean distance to galaxy pair $D_{\rm ave}$):

$$D_{ij} = 2D_{\rm ave}\sin(\Theta_{ij}/2) \le D_{\rm L}(D_{\rm ave}, f), \tag{4}$$

where

$$D_{\rm ave} \equiv (D(z_i) + D(z_j))/2; \tag{5}$$

and

$$V_{ij} = c \times |z_i - z_j| \le V_{\rm L}(D_{\rm ave}, f). \tag{6}$$

The distances $D(z)$ are comoving,

$$D(z) = \frac{c}{H_0 q_0^2 (1+z)}[q_0 z + (q_0 - 1)(\sqrt{2q_0 z + 1} - 1)] \tag{7}$$

($q_0 = 0.5$ and $H_0 = h \times 100$ km s^{-1} Mpc^{-1}). The variable Θ_{ij} is the angular separation between the two galaxies. If no companions are found within $D_{\rm L}$ and $V_{\rm L}$ of the seed galaxy, it is assigned "isolated" status and another seed galaxy is sought. If companions are found, they are added along with the seed galaxy to a list of group members forming a new group. In turn, the surroundings of each of these companions are combed for the next level of "friends." This loop is repeated until no further companions are located, and the process is begun again by pursuing another seed galaxy. The group catalogue is complete only once every galaxy in the redshift sample has been classified as either "isolated" or "grouped." Only those groups containing three or more members are included in the final catalogue.

The linking parameters, $D_{\rm L}$ and $V_{\rm L}$, are specified in a manner which compensates for both the radial selection function and the field-to-field sampling variations characteristic of the LCRS. For each pair of galaxies,

$$D_{\rm L} = D_0 \times S_{\rm L} \qquad \text{and} \qquad V_{\rm L} = V_0 \times S_{\rm L}, \tag{8}$$

where D_0 and V_0 are $D_{\rm L}$ and $V_{\rm L}$, respectively, for a given fiducial field at given fiducial redshift, and where $S_{\rm L}$ is a linking scale which takes into account variations in galaxy sampling rate. It is defined by

$$S_{\rm L} \equiv \left[\frac{n^{\rm exp}(f, D_{\rm ave})}{n^{\rm exp}_{\rm fid}}\right]^{-1/3}, \tag{9}$$

where $n^{\rm exp}(f, D_{\rm ave})$ is the number density of galaxies one would expect to observe at a comoving distance $D_{\rm ave}$ in field f for a randomly homogeneous distribution of galaxies having the same selection function and sampling fraction as the LCRS redshift catalogue; $n^{\rm exp}_{\rm fid}$ is $n^{\rm exp}(f, D_{\rm ave})$ for a given fiducial field at a given fiducial redshift (Fig. 2). Both $n^{\rm exp}_{\rm fid}$ and $n^{\rm exp}(f, D_{\rm ave})$ are computed by numerically integrating the field's selection function (see Appendix A).

To elaborate, the fiducial field is an idealized field with a given set of characteristics. The fiducial field is itself never generated. It merely serves as the basis for the normalization of the linking scale $S_{\rm L}$ in Equation 9. For simplicity, we have chosen our fiducial field to have 100% sampling, flux limits of $15.0 \le R < 17.7$, and a Schechter (1976) luminosity function with the same parameter values as the LCRS 112-fiber sample:

$$\alpha = -0.70, M^* = -20.29 + 5\log h, \phi^* = 0.019h^3 \text{ Mpc}^{-3} \tag{10}$$

(Lin et al. 1996). Since it is roughly the median redshift of the survey, we have chosen the fiducial redshift $cz_{\rm fid}$ to be 30,000 km s^{-1}.

Moving on, we note that field-to-field sampling variations are of particular concern when linking occurs across a field border. This concern is especially important in the case of a group situated on the border between a 50-fiber field and a 112-fiber field, where a factor of 2 discontinuity can occur in the expected surface density of galaxies on the sky. (Fortunately, only $\sim 2\%$ of the groups in the final catalogue — 28 out of 1495 — straddle a 50/112 border.) Therefore, when calculating the linking scale $S_{\rm L}$ for two galaxies in two different fields, $n^{\rm exp}(f, D_{\rm ave})$ is taken to be its average from the two fields,

$$n^{\rm exp}(f, D_{\rm ave}) \Longleftarrow (n^{\rm exp}(f_1, D_{\rm ave}) + n^{\rm exp}(f_2, D_{\rm ave}))/2. \tag{11}$$

But what of the artificial splitting of groups due to the LCRS's 55 arcsec fiber separation limit? To avoid this problem, each of the $\sim 1,000$ galaxies originally excluded from LCRS redshift catalogue due to the fiber separation limit has been re-introduced into the sample by assigning it a redshift equal to that of its nearest neighbor convolved with a gaussian of width $\sigma = 200$ km s^{-1} (roughly the median line-of-sight velocity dispersion of a cleaned LCRS group sample which excludes the 55-arcsec "orphans"). The re-included galaxies subscribe to all the same photometric limits and spatial borders that are imposed upon the original galaxy sample (§ 2).

In closing, we note that, for a given choice of D_0 and V_0, this algorithm leads to a unique group catalogue independent of the choice of the original seed galaxy. Due to the aforementioned field-to-field variations in sampling, however, it is more intuitive to characterize a group catalogue extracted from the LCRS not with D_0 for a certain fiducial field, but with

$$\frac{\delta n}{n} = \frac{3}{4\pi D_0^3 n_{\rm fid}^{\rm exp}} - 1, \tag{12}$$

the corresponding number density enhancement of the surface contour which delimits each group; the value $\delta n/n$ characterizes the groups more generally, as it is valid no matter the field in which a given group resides.

3.2. The Choice of Linking Parameters

So far, it has been shown how the superstructure of the group-finding algorithm has been set into place. The choice of values for $\delta n/n$ (D_0) and V_0, however, has yet to be presented and explained. We shall follow a course very similar to that of HG82 in our justification of the two values ultimately adopted.

Take Figure 3 as a guide to the choice of $\delta n/n$ (D_0) and V_0. Their selection should satisfy a few basic criteria. First, the density enhancement contour sought should be high enough to limit the number of interloper galaxies contained within a group, but not so high that only the cores of rich clusters are found. On the other hand, for a thin-wedge geometry like that of an LCRS slice, the groups selected should not be too loose; otherwise, edge effects become excessive. Furthermore, the value of V_0, as with the value of $\delta n/n$ (D_0), should minimize the number of interlopers, but without biasing group line-of-sight velocity dispersions toward artificially low values. As a definite upper limit, V_0 should not exceed the radius (in km s^{-1}) of a typical void observed at $cz_{\rm fid}$. The range of acceptable values for $\delta n/n$ (D_0) and V_0 are enclosed by the solid border in Figure 3. By means of the following semi-quantitative arguments, it will be concluded that the most reasonable values for the two linking parameters are

$$\delta n/n = 80 \quad (\Longleftrightarrow D_0 = 0.715\ h^{-1}\ \mathrm{Mpc}) \quad \text{and} \quad V_0 = 500\ \mathrm{km\ s^{-1}}, \tag{13}$$

which are denoted in Figure 3 by an asterisk.

First, consider the number of interlopers per galaxy, $n_{\rm I}$, within a specified $D_{\rm L}$ and $V_{\rm L}$ of some galaxy. For a given galaxy, $n_{\rm I}$ can be roughly estimated by the equation (HG82)

$$n_{\rm I} = \pi \left(\frac{D_{\rm L}}{D(z)} \right)^2 \left[\frac{N_{V_{\rm L}}(cz)}{N_{\rm tot}} \right] \Sigma_{\rm gal}, \tag{14}$$

where $\Sigma_{\rm gal}$ is the surface number density of galaxies in the redshift catalogue, $N_{\rm tot}$ is the total number of galaxies in the sample, and $N_{V_{\rm L}}(cz)$ is the number of galaxies within $V_{\rm L}$ of the galaxy's velocity cz. (This measure is actually an underestimate of $n_{\rm I}$, since it neglects the correlation of galaxy positions on the sky, but, if we stringently limit the number of interlopers per galaxy, it is adequate for our purposes.) The lower curve in Figure 3 denotes the locus $n_{\rm I} = 1$ for the the fiducial field at the fiducial redshift $cz_{\rm fid} = 30{,}000$ km s^{-1}. Below and to the right of this curve, where $n_{\rm I} > 1$, the number of interlopers per galaxy is considered excessive, and thus this curve constitutes one of our boundaries. Figure 4 presents $n_{\rm I}$ for the redshift of each galaxy in the LCRS sample for the values of $\delta n/n$ (D_0) and V_0 listed in equation 13. The bumps and dips in Figure 4 are due to inhomogeneities within the distribution of galaxy velocities (the wall-like structures) in the LCRS (Shectman et al. 1996). Note that the median number of interlopers per galaxy $n_{\rm I} \approx 0.2$ for our eventual choice of $\delta n/n$ (D_0) and V_0. There is only a slight large-scale trend evident in Figure 4, the fact of which argues that the number of spurious groups in the final catalogue should not be a strong function of redshift.

To preclude only finding the dense central regions of rich clusters, an arbitrary upper limit to the density enhancement contour cut is set at $\delta n/n = 200$, equivalent to assigning a value of 0.528 h^{-1} Mpc to D_0. In the quest for a catalogue of loose groups, a lower density contrast cutoff is preferred. Upon testing, it was discovered that, below a contrast of $\delta n/n = 80$, edge effects become a problem. At these cutoffs, over half of the groups must be excluded from the clean sample used in the study of group properties; the group radii encroach upon the slice's borders. Thus, the density contrast $\delta n/n = 80$ was chosen for the group catalogue, since it provides a reasonable compromise between the pursuit of loose groups and the desire for a large clean sample.

Next, the value of V_0 should be chosen such that group velocity dispersions are not overconstrained. To avoid seriously underestimating group velocity dispersions, we must set V_0 to a value which accommodates the maximum *likely* physical velocity dispersion, $\sigma_{\rm los}^{\rm max,phys}$. Mathematically, the maximum *possible* velocity dispersion of a group, $\sigma_{\rm los}^{\rm max,th}$, is that obtained when the group is maximally spread out in redshift — i.e., when each group member is just within the linking velocity $V_{\rm L}$ of its nearest neighbor:

$$\sigma_{\rm los}^{\rm max,th}(N_{\rm obs}, V_{\rm L}) = \frac{V_{\rm L}}{\sqrt{(N_{\rm obs}-1)}} \left[\sum_{i=1}^{N_{\rm obs}} \left(i - \frac{N_{\rm obs}+1}{2} \right)^2 \right]^{\frac{1}{2}}. \tag{15}$$

For example, the maximum velocity dispersion possible for a group containing $N_{\rm obs} = 10$ galaxies would be

$$\sigma_{\rm los}^{\rm max,th}(N_{\rm obs} = 10, V_{\rm L}) \approx 3.03 V_{\rm L}. \tag{16}$$

At the very least, we want this theoretical maximum *possible* velocity dispersion to encompass — i.e., to be greater than — the maximum *likely* physical velocity dispersion. Due to the LCRS galaxy selection function, a group containing $N_{\rm obs} = 10$ galaxies in a fiducial field at the fiducial velocity ($cz_{\rm fid}$ =30,000 km s^{-1}) will typically be of Abell richness class $R \approx 0$ (Abell 1958). If we make the conservative assumption that the maximum likely $\sigma_{\rm los}$ for a physical $R \approx 0$ "group" is no more than about $1,200$ km s^{-1} (Zabludoff et al. 1993; RPG97), we can set a lower limit for V_0 by means of the relation

$$\sigma_{\rm los}^{\rm max,th}(N_{\rm obs} = 10, cz = 30,000 \text{ km s}^{-1}) \gtrsim \sigma_{\rm los}^{\rm max,phys} \approx 1,200 \text{ km s}^{-1}, \tag{17}$$

which yields $V_0 \gtrsim 400$ km s^{-1}. This value provides the leftmost boundary to the region of acceptable $(\delta n/n, V_0)$ in Figure 3. At the other extreme, the velocity linking parameter should not be so large that galaxies are linked across a void diameter. Thus, we give V_0 a maximum limit equal to the typical radius of observed voids near $cz_{\rm fid}$ = 30,000 km s^{-1}, or $V_0 \lesssim 2000$ km s^{-1}. This maximum V_0 provides the rightmost border in Figure 3. To fine-tune V_0, the group algorithm was run, using $\delta n/n = 80$, for four different values: $V_0 =$ 500 km s^{-1}, $V_0 = 1000$ km s^{-1}, $V_0 = 1500$ km s^{-1}, and $V_0 = 2000$ km s^{-1} (Fig. 5). Many of the group velocity dispersions are unaffected by the change in V_0, but a significant number of groups, by adding progressively more outlying galaxies, see a dramatic increase in $\sigma_{\rm los}$ as V_0 is increased from 500 km s^{-1} to 2000 km s^{-1}. In the end, $V_0 = 500$ km s^{-1} was chosen, due to its lower probability of incorporating spurious groups into the catalogue, and due to its ability to generate a catalogue with a relatively low redshift-dependence in $\sigma_{\rm los}$. This latter property especially makes for a more homogeneous group sample.

4. The Group Catalogue

The full catalogue contains 1495 groups and includes 35% of the LCRS galaxy sample (Figs. 6, 7, & 8). The complete list of LCRS groups and their individual properties is compiled in Table 1, which, due to its size, is confined to the electronic version of this text.

Members of the clean sample of 394 groups — those which have barycenters more than two pairwise separations [column (12)] from a slice edge, crossing times [column (16)] less than a Hubble time, corrected line-of-sight velocity dispersions [column (9)] greater than zero, and no 55-arcsec "orphan" galaxies as group members — are marked by an asterisk in column (1). Group properties are calculated according to the prescriptions of RGH89, but modified for use with comoving distances and field-to-field sampling variations.

Before we enter a description of the tabulated group properties, we must note two caveats. First, even the clean sample is unlikely to be perfectly clean. As noted, one of the rejection criteria used is the removal of groups which are closer than two pairwise separations from a slice edge. In doing so, we have followed the lead of RGH89, who used this same rejection criterion to define their clean group sample. Clearly, having no "edge-proximity" rejection criterion would include many groups which overflow the survey boundaries. The measured properties of these groups would be biased from their true values due to their truncated membership. Since the pairwise separation, $R_{\rm p}$, is a measure of the group radius, excluding groups which are closer than one $R_{\rm p}$ to a slice edge should go far in counteracting this effect. One must be careful, though, since a truncated membership will both offset the position of the measured group barycenter away from the slice edge and bias the measure of $R_{\rm p}$ itself toward small values. Thus, a group which in fact extends over a slice border could still be accidentally included in the clean sample. Therefore, choosing an edge-proximity rejection criterion of $2 \times R_{\rm p}$ — although still not perfect — is much safer. One could even make more stringent demands, requiring groups in the clean sample to be at least three or four times their measured $R_{\rm p}$ from a slice edge. Here, however, one must worry about biasing the clean sample unnecessarily towards only the most compact systems. In Table 2, we see the effects of steadily increasing the threshold of edge-proximity rejection on the resulting clean samples: although the sample line-of-sight velocity dispersion, $\sigma_{\rm los}$, is not strongly affected, the sample pairwise separation and harmonic radius [$R_{\rm h}$; see column (14) of Table 1] both drop precipitously for these larger values of the rejection criterion. Therefore, as a compromise, we have chosen a value of $2 \times R_{\rm p}$.

Our second caveat is that the clean sample is not necessarily the best sample to use for all purposes. Since the clean sample excludes groups containing 55-arcsec "orphans", on average this sample discriminates against groups with dense cores. On some occasions (as in § 6), a superset of the clean sample – one which does not exclude groups merely because they harbor an "orphan" – is the preferred catalogue. The clean sample, as defined, however, is the most conservative catalogue – the sample with the fewest extrinsic assumptions attached to it. Therefore, in matters of discussing intrinsic mean group properties, we shall use this clean group sample.

With these caveats in mind, the columns in Table 1 are as follows:

Column (1): A running group identification number, $N_{\rm grp}$, for a given LCRS slice. The slice declination and $N_{\rm grp}$ form the basis of the IAU-registered naming convention for LCRS loose groups, which is of the form

$$\mathrm{LCLG}\ \ -DD\ NNN,$$

where LCLG stands for "Las Campanas Loose Group," $-DD$ is the (zero-padded) declination for the LCRS slice wherein the group resides, and NNN is the (zero-padded) $N_{\rm grp}$. For more information, see the online Dictionary of Nomenclature of Celestial Objects (`http://cdsweb.u-strasbg.fr/cgi-bin/Dic`).

An asterisk appended to $N_{\rm grp}$ in Table 1 indicates that the group is a member of the clean sample.

Columns (2 – 4): A weighted measure of the B1950.0 right ascension (in HH MM SS.ss format) of the group's barycenter,

$$\alpha_{1950.0} = \frac{\sum_{i=1}^{N_{\rm obs}} w_i \alpha_i}{\sum_{i=1}^{N_{\rm obs}} w_i}, \tag{18}$$

where

$$w_i \equiv \frac{1}{n^{\rm exp}(f_i, D(z_i))} \tag{19}$$

This weighting factor — which is proportional to the inverse of the selection function — helps to counteract a bias resulting from a group straddling two fields with different galaxy sampling characteristics; a discussion on how $n^{\rm exp}(f_i, D(z_i))$ is estimated can be found in Appendix A. $N_{\rm obs}$, the number of observed group members, is listed in column (11).

Column (5-7): A weighted measure of the B1950.0 declination (in sDD MM SS.s format) of the group's barycenter,

$$\delta_{1950.0} = \frac{\sum_{i=1}^{N_{\rm obs}} w_i \delta_i}{\sum_{i=1}^{N_{\rm obs}} w_i}, \tag{20}$$

where w_i is as defined in equation 19. $N_{\rm obs}$ is listed in column (11).

Column (8): The group's redshift, $z_{\rm cmb}$, with respect to the local comoving frame. It is taken as the (unweighted) mean of the members' redshifts. (See Figs. 9 & 10.)

Column (9): The group line-of-sight velocity dispersion, in km s^{-1}, corrected for relativistic effects (Harrision 1974),

$$\sigma_{\rm los} = \frac{1}{1+ < z >} \sqrt{\frac{\sum_{i=1}^{N_{\rm obs}} (cz_i - < cz >)^2}{(N_{\rm obs} - 1)}} \tag{21}$$

(Fig. 11). The random errors in the LCRS galaxy redshift measurments are also removed, in quadrature, assuming $\sigma_{cz} = 67$ km s^{-1} (Shectman et al. 1996):

$$\sigma_{\rm los} \Longleftarrow \begin{cases} \sqrt{\sigma_{\rm los}^2 - (67 \text{ km s}^{-1})^2}, & \text{if } \sigma_{\rm los} > 67 \text{ km s}^{-1} \; ; \\ 0, & \text{otherwise.} \end{cases} \tag{22}$$

$N_{\rm obs}$ is listed in column (11).

Column (10): A formal estimate of the standard error in $\sigma_{\rm los}$, in km s^{-1}. If a normal distribution is assumed for the line-of-sight velocities, the standard error for $\sigma_{\rm los}^2$ can be expressed as

$$\sigma(\sigma_{\rm los}^2) = \sigma_{\rm los}^2 \sqrt{\frac{2}{N_{\rm obs}}\left(1 - \frac{1}{N_{\rm obs}}\right)} \tag{23}$$

(Deming 1950). By means of propagation of errors (Bevington 1969), this expression yields

$$\sigma(\sigma_{\rm los}) = \frac{1}{2}\sigma_{\rm los} \sqrt{\frac{2}{N_{\rm obs}}\left(1 - \frac{1}{N_{\rm obs}}\right)}, \tag{24}$$

which is employed for the estimates listed in Column (10). $N_{\rm obs}$ is listed in column (11).

Column (11): $N_{\rm obs}$, the observed number of LCRS galaxies (including any 55-arcsec "orphans") comprising the group (Fig. 12). Included in $N_{\rm obs}$ are only those LCRS galaxies which the lie within the official geometric and photometric borders of the survey and which subscribe to the redshift and absolute magntitude limits set forth in equations 1 and 2.

As is typical for "friends-of-friends" group catalogues, the distribution of $N_{\rm obs}$ for the LCRS group catalogue is heavily skewed toward small values: the median $N_{\rm obs}$ is 3.

Column (12): The mean pairwise separation,

$$R_{\rm p} = \frac{8 D_{\rm grp}}{\pi} \sin\left[\frac{1}{2} < \theta_{ij} >\right], \tag{25}$$

where

$$< \theta_{ij} > \equiv \frac{\sum_i \sum_{j>i} w_i w_j \theta_{ij}}{\sum_i \sum_{j>i} w_i w_j}, \tag{26}$$

and where $D_{\rm grp}$ is the comoving distance to the group, θ_{ij} is the angular separation between group members i and j, and w_i and w_j are the respective weights for i and j (equation 19). $R_{\rm p}$ has dimensions h^{-1} Mpc. See Figure 13.

Column (13): An estimate of the rms error in $R_{\rm p}$,

$$\sigma_{R_{\rm p}} = \left(\frac{4}{\pi}\right) D_{\rm grp} \sigma_{<\theta_{ij}>}, \tag{27}$$

where

$$\sigma_{<\theta_{ij}>} = \sqrt{\frac{N_{\rm pair} \sum_i \sum_{j>i} (w_i w_j \theta_{ij})^2 - \left(\sum_i \sum_{j>i} w_i w_j \theta_{ij}\right)^2}{(N_{\rm pair}-1)\left(\sum_i \sum_{j>i} w_i w_j\right)^2}}, \tag{28}$$

where $N_{\rm pair}$ is the number of distinct galaxy pairs in the group, and where $D_{\rm grp}$, θ_{ij}, w_i, and w_j are as described for $R_{\rm p}$ (equations 25 and 26).

Equation 27 was derived from Equation 25, assuming that $\sin(0.5 <\theta_{ij}>) \approx 0.5 <\theta_{ij}>$ for the typical group angular sizes encountered in this group catalogue, and that the contribution to $\sigma_{R_{\rm p}}$ by the rms error in $D_{\rm grp}$ is insignificant compared to the contribution by $<\theta_{ij}>$. Equation 28 was derived from equation 26 via a straightforward (albeit tedious) application of propagation of errors.

The units for $\sigma_{R_{\rm p}}$ are h^{-1} Mpc.

Column (14): The harmonic radius,

$$R_{\rm h} = \pi D_{\rm grp} \sin\left[\frac{1}{2} < \theta_{ij}^{-1} >^{-1}\right], \tag{29}$$

where

$$< \theta_{ij}^{-1} > \equiv \frac{\sum_i \sum_{j>i} w_i w_j \theta_{ij}^{-1}}{\sum_i \sum_{j>i} w_i w_j}. \tag{30}$$

$D_{\rm grp}$, θ_{ij}, and w_i and w_j are as described for $R_{\rm p}$ (equations 25 and 26). $R_{\rm h}$ has dimensions h^{-1} Mpc. See Figure 14.

Column (15): An estimate of the rms error in $R_{\rm h}$,

$$\sigma_{R_{\rm h}} = \left(\frac{\pi}{2}\right)\left(\frac{D_{\rm grp}}{< \theta_{ij}^{-1} >^2}\right)\sigma_{<\theta_{ij}^{-1}>}, \tag{31}$$

where

$$\sigma_{<\theta_{ij}^{-1}>} = \sqrt{\frac{N_{\rm pair} \sum_i \sum_{j>i} \left(w_i w_j \theta_{ij}^{-1}\right)^2 - \left(\sum_i \sum_{j>i} w_i w_j \theta_{ij}^{-1}\right)^2}{(N_{\rm pair}-1)\left(\sum_i \sum_{j>i} w_i w_j\right)^2}}. \tag{32}$$

$N_{\rm pair}$ is the number of distinct galaxy pairs in the group; $D_{\rm grp}$, θ_{ij}, w_i, and w_j are as described for $R_{\rm p}$ (equations 25 and 26).

The derivation of equations 31 and 32 closely mimics that of equations 27 and 28.

The units for $\sigma_{R_{\rm h}}$ are h^{-1} Mpc.

Column (16): The crossing time for the group,

$$t_{\rm cr} = \frac{3}{5^{3/2}} \frac{R_{\rm h}}{\sigma_{\rm los}}, \tag{33}$$

in units of the Hubble time (H_0^{-1}); see Figure 15. This measure is heavily influenced by the relative values of the linking parameters D_0 (which determines $R_{\rm h}$) and V_0 (which determines $\sigma_{\rm los}$). Following Gott & Turner (1977), it can be estimated that the time for a uniform sphere to undergo complete virialization is

$$t_{\rm vir} \sim 3\pi t_{\rm cr}. \tag{34}$$

Hence, all groups with $t_{\rm cr} \lesssim 0.11 H_0^{-1}$ should have had enough time to virialize completely within the age of the Universe [but see Diaferio et al. (1993)]. Thus, it can be deduced that roughly half of the LCRS clean sample could have undergone complete virialization.

Column (17): An estimate of the rms error in $t_{\rm cr}$,

$$\sigma_{t_{\rm cr}} = t_{\rm cr}\sqrt{\frac{\sigma_{R_{\rm h}}^2}{R_{\rm h}^2} + \frac{\sigma_{\sigma_{\rm los}}^2}{\sigma_{\rm los}^2}}, \tag{35}$$

in units of the Hubble time (H_0^{-1}); $\sigma_{\rm los}$, $\sigma_{\sigma_{\rm los}}$, $R_{\rm h}$, and $\sigma_{R_{\rm h}}$ come from columns (9), (10), (14), and (15), respectively. Equation 35 was derived by standard propagation of errors analysis of equation 33.

Column (18): The group's virial mass,

$$M_{\rm vir} = \frac{6\sigma_{\rm los}^2 R_{\rm h}}{G}, \tag{36}$$

where G is the gravitational constant (Fig. 16). This estimate assumes that the groups are virialized and that the galaxies trace the mass distribution within the group [see, for example, Binney & Tremaine (1987), Chapter 10, Section 2.3]. $M_{\rm vir}$ is in units of $h^{-1}\ M_\odot$.

Column (19): An estimate of the rms error in $M_{\rm vir}$,

$$\sigma_{M_{\rm vir}} = M_{\rm vir}\sqrt{\frac{4\sigma_{\sigma_{\rm los}}^2}{\sigma_{\rm los}^2} + \frac{\sigma_{R_{\rm h}}^2}{R_{\rm h}^2}}, \tag{37}$$

where $\sigma_{\rm los}$, $\sigma_{\sigma_{\rm los}}$, $R_{\rm h}$, and $\sigma_{R_{\rm h}}$ come from columns (9), (10), (14), and (15), respectively. Equation 37 was derived by propagation of errors analysis of equation 36. Note that the large random errors inherent to $\sigma_{\rm los}$ and to $R_{\rm h}$ propagate into estimates for $M_{\rm vir}$. The units for $\sigma_{M_{\rm vir}}$ are $h^{-1}\ M_\odot$.

Column (20): The total group luminosity in the LCRS R-band, $L_{\rm tot}$, corrected for selection effects to account for galaxies not observed by the LCRS (Fig. 17); $L_{\rm tot}$ is in units of solar luminosity ($h^{-2}\ L_\odot$), in which the R-band absolute magnitude of the Sun is taken to be

$M_{R;\odot} = +4.52$ (Pinsonneault 1992). The mathematical apparatus behind the correction factor can be found in Appendix B.

Column (21): An estimate of the rms error in $L_{\rm tot}$, $\sigma_{L_{\rm tot}}$, obtained by summing the rms errors of the individual components of $L_{\rm tot}$ in quadrature. Details can be found in Appendix B. The units for $\sigma_{L_{\rm tot}}$ are $h^{-2}\ L_\odot$ (LCRS R-band).

Column (22): The ratio, $L_{\rm rat}$, by which the sum of the luminosities of the observed $N_{\rm obs}$ galaxies must be multiplied in order to obtain an estimate of the group's total (LCRS R-band) luminosity, $L_{\rm tot}$,

$$L_{\rm rat} \equiv \frac{L_{\rm tot}}{\sum_{i=1}^{N_{\rm obs}} L_i} \tag{38}$$

Over the clean sample, the median $L_{\rm rat}$ is ≈ 5.4 for the 50-fiber groups and ≈ 2.4 for the 112-fiber groups.

Column (23): The group mass-to-light ratio in the LCRS R-band, M/L, in units of $h\ M_\odot/L_\odot$ (Fig. 18). For comparison with the mass-to-light ratios for groups from other redshift catalogues (in particular, those based upon the de Vaucouleurs $B(0)$-band), it is convenient to note that

$$M/L_{B(0)} \sim 1.1 M/L \text{ (LCRS)}. \tag{39}$$

The uncertainties in $M_{\rm vir}$ and in $L_{\rm tot}$ tend to give large errors for the mass-to-light ratios of individual groups.

Column (24): An estimate of the rms error in M/L,

$$\sigma_{M/L} = \left(\frac{M}{L}\right)\sqrt{\frac{\sigma^2_{M_{\rm vir}}}{M^2_{\rm vir}} + \frac{\sigma^2_{L_{\rm tot}}}{L^2_{\rm tot}}} \tag{40}$$

where $M_{\rm vir}$, $\sigma_{M_{\rm vir}}$, $L_{\rm tot}$, and $\sigma_{L_{\rm tot}}$ come from columns (18), (19), (20), and (21), respectively. Equation 40 was obtained by means of propagation of errors analysis of equation 39. The units for $\sigma_{M/L}$ are $h\ M_\odot/L_\odot$.

Column (25): An estimate of the group's Abell counts, $C_{\rm grp}$ (Fig. 19). Abell (1958) defined his counts to be the number of galaxies, corrected for background contamination, in the magnitude interval m_3 to $m_3 + 2$, that lie within a 1.5 h^{-1} Mpc projected separation of a cluster's center; the magnitude m_3 is the magnitude of the third brightest cluster member. Due to the sampling characteristics and the relatively small range of apparent magnitudes within the LCRS, we could not use Abell's definition directly. We had instead to derive each group's Abell counts via a Schechter function; the details of the method can be found in Appendix C. When compared with actual Abell clusters within the LCRS volume (§ 6), we find the following relation between the LCRS group counts estimate, $C_{\rm grp}$, and the revised Abell cluster values given by ACO:

$$C_{\rm grp} \sim 0.19 C_{\rm ACO} + 12. \tag{41}$$

Column (26): An estimate of the error in the Abell counts $C_{\rm grp}$, based upon Poisson statistics of the observed number of LCRS member galaxies within a projected distance of 1.5 h^{-1} Mpc of the group center ($N_{\rm obs}^{1.5}$),

$$\sigma_{C_{\rm grp}} \sim \frac{C_{\rm grp}}{\sqrt{N_{\rm obs}^{1.5}}}. \tag{42}$$

Column (27): The type of group — one within the borders of a 50-fiber field (Type 1), one within the borders of a 112-fiber field (Type 2), or one straddling the border of a 50- and a 112-fiber field (Type 3).

Column (28): A column to reference any applicable notes for the given group. These table notes are as follows:

a: the group's crossing time $t_{\rm cr}$ is greater than a Hubble time (H_0^{-1}).

b: the group's barycenter is closer than $2R_{\rm p}$ to a slice edge.

c: the group contains at least one 55 arcsec "orphan" with a mock redshift.

d: the group's line-of-sight velocity dispersion, corrected for galaxy velocity errors, is less than or equal to 0 km s^{-1}.

Table 3 lists the members of each group. Due to its great size (10761 lines), it is provided only in electronic format. Each group is introduced by a header composed of its group number designation $N_{\rm grp}$, its redshift $z_{\rm cmb}$, and its line-of-sight velocity dispersion $\sigma_{\rm los}$ [Columns (1), (8), and (9) of Table 1, respectively]. The columns for Table 2 are as follows:

Column (1): A group member identification number.

Columns (2-4): The group member's right ascension in 1950.0 coordinates.

Columns (5-7): The group member's declination in 1950.0 coordinates.

Column (8): The group member's LCRS R-band isophotal magnitude.

Column (9): The group member's LCRS R-band central magnitude.

Column (10): The group member's heliocentric velocity, $cz_{\rm helio}$, in km s^{-1}.

Column (11): The group member's spectrum type (e = contains strong emission lines; c = a continuum with absorption lines; b = contains both absorption lines and moderate emission lines; m = mock velocity — i.e., the galaxy was one of the 55-arcsec "orphans" excluded from the spectroscopic survey due to its proximity to another galaxy).

The individual group member properties are derived directly from a working copy of the published LCRS galaxy catalogue; further details can be found in Shectman et al. (1996).

5. Comparison of Various Group Catalogues

Table 4 contains information regarding the general properties of groups both in the LCRS catalogue and from other catalogues. The values tabulated for the eight non-LCRS group catalogues have been taken from the original papers, and, where necessary, these values were converted to be consistent with the property definitions detailed in § 4. The median properties for the LCRS catalogue were derived from the clean sample of 394 groups; the fraction of grouped galaxies, from the full sample of 1495 groups.

5.1. LCRS Group Catalogues

We have broken the LCRS groups catalogue into three sub-catalogues for the purpose of inter-comparison; the sub-catalogues include the LCRS groups from 50-fiber fields, the LCRS groups from 112-fiber fields, and the LCRS groups which straddle a 50/112 border. Furthermore, we can compare the present LCRS group catalogue with a precursor based upon the LCRS -6° slice (Tucker 1994; henceforth, T94). The properties of these LCRS group samples are tabulated under the LCRS main heading in Table 4.

Note that there is substantial variation in group properties among the three sub-catalogues. These variations are also apparent in Figures 11 – 19. First, we can discount the oddities apparent in the 50/112 group properties due to poor number statistics (there are only 5 of these groups in the clean sample) and due to the difficulties of linking group members across a 50/112 border. In any case, if not for its aberrantly large $\sigma_{\rm los}$'s — which in turn affect estimates of $M_{\rm vir}$ and M/L — the 50/112 sample properties would closely match those of the 50-fiber sample. Unfortunately, the discrepancies between the 50- and the 112-fiber samples' group properties are somewhat harder to dismiss. Great effort was put forth into accounting for field-to-field sampling variations in the group-finding algorithm, including using appropriate luminosity functions and surface brightness cutoff functions for each of the northern 50-fiber, the southern 50-fiber, the northern 112-fiber, and the southern 112-fiber field types (Lin et al. 1996). Apparently, some small residual selection bias between the 50- and 112-fields remains. Fortunately, we can still follow one of two options: (1) we can choose to ignore the 50-fiber groups altogether (they make up only $\approx 20\%$ of the total number of groups), or (2) we can note that both the 50-fiber and the 112-fiber group properties fall within the general range of typical group properties from other surveys (§ 5.2) and thus consider the combined LCRS group catalogue as being representative of groups as a whole. Unless otherwise noted, we will take the latter course in the following sections.

Finally, consider the properties from an earlier version of the LCRS group catalogue (T94). This group catalogue is composed of only 50-fiber data from the LCRS -6° slice, so it is not surprising that many of its general properties have values which approximate those of the present 50-fiber sample. One major difference is the percentage of galaxies in groups. The relatively small value for the T94 sample may be attributed at least in part to the fact that the earlier LCRS group-finding algorithm ignored 55-arcsec "orphans," thus disrupting many groups into doublets or isolated galaxies which were excluded from the resulting T94 catalogue.

5.2. Group Catalogues from Other Redshift Surveys

It is instructive to compare the LCRS group catalogue with those derived from other galaxy redshift surveys. In this section we shall look at nine other group catalogues extracted from five different surveys and relate their properties to those of LCRS groups. The nine group catalogues considered are those by GH83, NW87, N93, MFW93, MdCL89, RGH89, RPG97, TB98, and RZZ99. The five surveys are the CfA1 (Huchra et al. 1983), the SSRS (da Costa et al. 1988,1991), the CfA2 (de Lapparent, Geller, & Huchra 1988; Huchra et al. 1990; Huchra, Geller, & Corwin 1995), the PPS (Giovannelli & Haynes 1993; Wegner, Haynes, & Giovanelli 1993), and the ESP (Vettolani et al. 1997). Table 5 summarizes the general properties of the different survey samples used to generate these group catalogues; for comparison, the characteristics of the LCRS sample used in this paper are also included (note that the LCRS sample contains substantially more galaxies and encloses the largest volume of any of the survey samples listed). The interested reader is urged to consult the original papers for details.

Now, as one might suspect from the small-but-statistically-significant differences between subsamples of the LCRS group catalogue (§ 5.1; Figs. 11 – 19), it is unlikely that another group catalogue — extracted from a different survey with different galaxy selection criteria using another variation of a "friends-of-friends" group-finding algorithm — would be from the same statistical parent population of groups as the LCRS group catalogue. To verify this, we have used the Kolmogorov-Smirnov (KS) Test to compare the physical properties of the LCRS groups with those of the five group catalogues available in machine-readable form (GH83, MdCL89, RPG97, TB98, and RZZ99). The results of our analysis are shown in Figures 21 – 27 and summarized in Table 6. Notice that most of the formal KS probabilities are so low that we needed to list them in logarithmic form in order to make Table 6 readable. Thus, these group catalogues are not extracted from the same parent population as the LCRS groups: their properties, although roughly similar (Table 4), do differ significantly.

There is a hidden benefit in these very low KS probabilities. The other four group catalogues are not available in machine-readable form (and two of those were not even published in paper form). Since these four have roughly the same number statistics and variations in physical properties as the other five, we can with some safety assume that the physical properties of the groups from these four catalogues also differ significantly from those of the LCRS group sample. We can therefore exploit the one statistic that is published for the properties of all nine of these group catalogues — the median — as a reasonable measure of comparison.

Now, in comparison with these other group catalogues, it is clear from Table 4 that the median properties of the full LCRS group catalogue (those under the "All" heading) are fairly typical. This is comforting, since it shows that all these group catalogues are looking at roughly the same sort of systems. But can more be said? Due to differing survey characteristics and differing group-extracting parameters, it is notoriously difficult to make cross-catalogue comparisons. Nonetheless, rough comparisons can be made.

Of the properties that Table 4 lists, two are primarily $D_{\rm L}$-dependent ($<R_{\rm h}>_{\rm med}$, $<R_{\rm p}>_{\rm med}$), one is primarily $V_{\rm L}$-dependant ($<\sigma_{los}>_{\rm med}$), and several are dependent in more-or-less complex ways on both $D_{\rm L}$ and $V_{\rm L}$ (# of groups in catalogue, # of groups in clean sample, % of galaxies in groups, $<H_0 t_{\rm cr}>_{\rm med}$, $<M_{\rm vir}>_{\rm med}$, $<L_{\rm tot}>_{\rm med}$, $<M/L>_{\rm med}$). Let us designate the properties which depend primarily only on $D_{\rm L}$ *or* $V_{\rm L}$ as *simply derived* properties, and those that depend more complexly on both $D_{\rm L}$ *and* $V_{\rm L}$ as *complexly derived* properties. Of the simply derived properties, those depending mainly on $D_{\rm L}$ can be considered density defining quantities; the one that mainly depends on $V_{\rm L}$ ($<\sigma_{los}>_{\rm med}$) defines the mean gravitational energy content of the systems. Many of the complexly derived properties are straightforward functions of combinations of the simply derived properties (see § 4).

Let us first consider the simply derived properties.

What can we say about the relative mean densities of the groups from the different catalogues? Consider $<R_{\rm h}>_{\rm med}$. For the catalogues which on average contain the denser groups, $<R_{\rm h}>_{\rm med}$ should be relatively small. Under this criterion, we find that the TB98 and RPG97 catalogues contain the densest systems on average; the LCRS, GH83, MdCL89, RGH89, and N93 catalogues, those of average density; and the NW87 catalogue, the least dense. $<R_{\rm p}>_{\rm med}$ is another indicator of relative group density, and, albeit with some changes in rank, roughly the same trend is seen. Thus, we can conclude that the TB98 and RPG97 groups are the densest on average; the LCRS, GH83, MdCL89, RGH89, and N93 groups are average systems; and the NW87 groups are the least dense.

Next, what can we infer about the mean gravitational energy content of the various catalogues — i.e, which are the "hottest" systems, the systems with the highest $<\sigma_{los}>_{\rm med}$? From Table 4, we see that the GH83 and RGH89 catalogues have high $<\sigma_{los}>_{\rm med}$, the LCRS, MdCL89, RPG97, TB98, and RZZ99 catalogues have intermediate values, and the NW87, N93, and MFW93 catalogues are the "coolest" of the systems listed (this is a reflection in part on the functional forms of the linking lengths used in NW87, N93, and MFW93, which strongly limit velocity outliers).

The values for the complexly derived quantities are by their very natures less certain. We will consider three specifically — $<M_{\rm vir}>_{\rm med}$, $<H_0 t_{\rm cr}>_{\rm med}$, and $<M/L>_{\rm med}$.

Consider $<M_{\rm vir}>_{\rm med}$: the GH83 and the RGH89 systems are the most massive, followed in order of decreasing mass by the LCRS, the RPG97, the MdCL89, the NW87, and the TB98 systems. It may seem strange that the catalogue containing the densest systems (TB98) is also the catalogue with the least massive systems. In fact, this is a consequence of the relatively small linking lengths $D_{\rm L}$ that TB98 used to extract his groups from the PPS: his groups do not extend out to the same radii as those in the "looser" catalogues, so they enclose less mass. On the other hand, his groups are the most virialized systems in Table 4 (based upon their short crossing times), so his catalogue estimate for $<M_{\rm vir}>$ is probably the most accurate. (The LCRS groups catalogue have a somewhat longer median crossing time, but one can still expect a large fraction of them to be virialized — see equation 34.)

We can also ask which group catalogues give evidence for the most (or least) dark matter. The LCRS group catalogue has a $<M/L>_{\rm med}$ of 171 h $M_{\odot}/L_{\odot}$ in the LCRS R-band; if we convert this to the de Vaucouleurs $B(0)$-band (equation 39) used by the other group catalogues with measured mass-to-light ratios, we find $<M/L>_{\rm med}$= 188 h $M_{\odot}/L_{\odot}$. This is fairly average. Of the other group catalogues with measured values of $<M/L>_{\rm med}$, the N93 and RGH89 catalogues show lower mass-to-light ratios, and the RPG97 and NW87 show higher.

In conclusion, we can state the LCRS group catalogue is quite average in its simply derived properties — its groups are of average density and gravitional energy content. Furthermore, it is not particularly distinct in its complexly derived properties — the groups being moderately massive with relatively long crossing times and average mass-to-light ratios. It is, however, a very large catalogue of groups in a wide variety of environments. The LCRS values for the properties tabulated here are among the least-biased presently available.

6. Abell Clusters in the LCRS Group Catalogue

The original Abell Catalogue (Abell 1958) is comprised of 2712 rich, highly dense clusters in the northern sky. Revised and expanded to include southern clusters, an updated Abell Catalogue (ACO) now contains 4073 rich clusters over a significant fraction of the whole sky. Each cluster contains within a projected radius of 1.7 arcmin/z ($\approx 1.5h^{-1}$ Mpc) from its center at least 30 member galaxies in the magnitude range m_3 to $m_3 + 2$, where m_3 is the apparent magnitude of the third brightest cluster member. The Abell/ACO catalogue nominally encompasses a redshift range of $0.02 \lesssim z \lesssim 0.20$; the redshifts are estimated empirically based upon the apparent magnitude of the tenth brightest member, m_{10}, and tend to be accurate to within a factor of 2. Each cluster is classified according to distance class D, estimated from m_{10}, and according to richness class R, based on the number of members meeting the above criteria for projected radial distance and apparent brightness. Furthermore, a supplementary catalogue of southern clusters too poor or too distant to be included in the main catalogue contains an additional 1174 clusters (Abell S001 – S1174).

How many Abell clusters do we expect to identify within the LCRS group catalogue? There are 206 Abell clusters (including those from the supplementary catalogue) within the sky-projected confines of the six LCRS slices. If we confine ourselves to a superset of the clean sample — one which includes groups with 55 arcsec “orphans” meeting the other criteria for inclusion into the clean sample — there are 735 LCRS loose groups which could be matched. The Abell catalogue is purported to be complete to a redshift of 0.20, but the LCRS group catalogue only goes to a redshift of 0.15; so we expect $\sim (0.15/0.20)^3 \sim {}^1\!/_2$ of Abell clusters to be lost due to distance. Furthermore, if we assume a typical pairwise separation of $R_\mathrm{p} \approx 0.6h^{-1}$ Mpc, the effective volume of the LCRS slices for the superset sample is again reduced by about half. Therefore, we expect about ${}^1\!/_2 \times {}^1\!/_2 \times 206 \approx 50$ matches between Abell clusters and LCRS groups.

We find 54 matches, which are described in Table 7. The columns are as follows:

Column (1): The LCRS group's running identification number for the given slice ($N_{\rm grp}$).

Column (2): The LCRS group's α in equinox 1950.0 coordinates ($\alpha_{\rm grp}$).

Column (3): The LCRS group's δ in equinox 1950.0 coordinates ($\delta_{\rm grp}$).

Column (4): The LCRS group's redshift ($z_{\rm grp}$).

Column (5): The observed number of galaxies from the LCRS official spectroscopic sample that lie within the group ($N_{\rm obs}$).

Column (6): An estimate of the Abell Richness for that group ($C_{\rm grp}$).

Column (7): The name of the Abell cluster match to this group.

Column (8): The Abell cluster's α in equinox 1950.0 coordinates ($\alpha_{\rm ACO}$).

Column (9): The Abell cluster's δ in equinox 1950.0 coordinates ($\delta_{\rm ACO}$).

Column (10): The Abell cluster's redshift ($z_{\rm ACO}$), if known.

Column (11): The Abell cluster's richness class (R).

Column (12): The Abell cluster's distance class (D).

Column (13): The Abell cluster's Abell counts, as measured by ACO ($C_{\rm ACO}$).

Column (14): The angular separation in arcminutes between the measured group center and the Abell cluster center as reported by ACO. A group-cluster pair was considered a "match" if this angular separation was less than 12 arcmin ($\sim 1\ h^{-1}$ Mpc at the median redshift of the LCRS).

Of these matches, we see that some are quite good ($N_{\rm obs} \geq 5$, separation $\lesssim 6$ arcmin, convergent cluster distance/group redshift, distance class < 6), such as the match between LCLG-42 010 and Abell 2758, and that others are not so good (separation $\gtrsim 6$ arcmin, widely divergent cluster distance/group redshift). Of the latter, some of the LCRS groups are likely in the foreground (LCLG-39 172, LCLG-39 202) or in the background (LCLG-03 126, LCLG-39 256, LCLG-42 052, LCLG-42 234). Furthermore, some Abell clusters have been split into two or more groups by the "friends-of-friends" algorithm (Abell 1200, S418, 2969, S281, S253, S286). All in all, however, the matchups are not too bad, especially for those groups with $N_{\rm obs} > 3$ observed members and those clusters of Abell distance class $D < 6$.

If we consider just the non-split $N_{\rm obs} > 3, D < 6$ matches, we find by least-squares fit that

$$C_{\mathrm{grp}} \sim 0.19 C_{\mathrm{ACO}} + 12$$

(eq. [41]; see Fig. 20). Such a poor correspondence between C_{grp} and C_{ACO} may be disheartening at first — at least until one realizes that independent measures of C_{ACO} among Abell, Corwin, and Olowin *themselves* often had random and systematic offsets of up to 50 galaxy counts (see ACO, Figs. 6 & 7). Furthermore, ACO stress that the measured counts for individual clusters are nearly meaningless. Therefore, we also stress that C_{grp} (or the corresponding C_{ACO} from eq. [31]) for individual LCRS groups will likely be very noisy; it is better to consider mean or median values of these estimates for sets of LCRS groups.

For instance, the median C_{grp} for LCRS groups is 10.8 (Fig. 19). This value for C_{grp} indicates a median $C_{\mathrm{ACO}} \sim -6$, which implies that LCRS groups, on average, can be thought of as very poor clusters. (The negative values for the median counts is based in part to the different means of background subtraction used here and in ACO.) Clearly, the LCRS groups do define an environment intermediate between that of isolated galaxies and that of rich clusters.

7. Summary and Conclusions

We have presented in this paper a catalogue of loose groups within the LCRS. These groups were extracted from the LCRS galaxy catalogue by means of a standard Huchra-Geller "friends-of-friends" percolation algorithm, modified for comoving distances and for the field-to-field sampling variations characteristic of this redshift survey.

Internal comparisons of characteristics within the LCRS group catalogue indicated some minor differences between groups extracted from the 50-fiber fields and those extracted from the 112-fiber fields. We attributed these differences to some small but still-hidden residual selection bias between galaxies in the 50-fiber and in the 112-fiber fields. Since groups in the 50-fiber sample comprise only $\approx 20\%$ of the LCRS group catalogue, and since the properties of both the 50-fiber and the 112-fiber groups fall within the general regime of other group catalogues, we found this discrepancy to be of only minor importance.

External comparison of the LCRS group catalogue with nine other group catalogues, all based upon other redshift surveys, showed that the general properties of LCRS groups are quite typical of current group catalogues. Nonetheless, it, along with the ESP group catalogue (RZZ99), is the only group catalogue based upon a redshift survey covering a reasonably fair sample of the local Universe. Therefore, the properties of the LCRS group catalogue, containing groups from a wide range of environments, should be among the least biased to date.

Matchups of the LCRS groups with Abell clusters indicated, not surprisingly, that, on average, these groups are much poorer than Abell-class clusters, and therefore that LCRS groups do indeed inhabit a range of parameter space intermediate to that of individual galaxies and to that of rich clusters.

We therefore conclude that this catalogue will be useful for a variety of studies requiring an unbiased census of loose groups, including the measurement of the luminosity function of group members versus that of field galaxies, the investigation of various morphology-environment relations, and the study of the clustering of groups.

We thank the anonymous referee for the many useful comments.

DLT would also like to thank Marcio Maia, Ben Moore, Richard Nolthenius, Massimo Ramella, and Roberto Trasarti-Battistoni for valuable discussions — by e-mail or in person — concerning their group catalogues.

The Las Campanas Redshift Survey has been supported by NSF grants AST 87-17207, AST 89-21326, and AST 92-20460. This research has made use of the NASA/IPAC Extragalactic Database (NED), which is operated by the Jet Propulsion Laboratory, Caltech, under contract with the National Aeronautics and Space Administration.

This work was supported in part by the US Department of Energy under contract No. DE-AC02-76CH03000.

A. Calculating $n^{\rm exp}(f,D)$ and $n^{\rm exp}_{\rm fid}$ for the LCRS

We estimate $n^{\rm exp}(f,D)$ via

$$n^{\rm exp}(f,D) = F \times \phi^* \int_{L_{\rm min}}^{L_{\rm max}} \left(\frac{L}{L^*}\right)^{\alpha} e^{-L/L^*} d\left(\frac{L}{L^*}\right). \tag{A1}$$

Equation A1 is just the Schechter (1976) luminosity function multiplied by a corrective factor F and integrated over the interval $L_{\rm min} \leq L \leq L_{\rm max}$. $L_{\rm min}$ and $L_{\rm max}$ are the extremal luminosities observable at a comoving distance D under the flux and luminosity limits imposed on field f, F is the field-to-field sampling fraction for field f, and ϕ^*, L^*, and α are the standard Schechter function parameters.

The value for $n^{\rm exp}_{\rm fid}$ is calculated in the same manner,

$$n^{\rm exp}_{\rm fid} = F \times \phi^* \int_{L_{\rm min}}^{L_{\rm max}} \left(\frac{L}{L^*}\right)^{\alpha} e^{-L/L^*} d\left(\frac{L}{L^*}\right), \tag{A2}$$

where the values for F, $L_{\rm min}$, $L_{\rm max}$, ϕ^*, L^*, and α are those for the fiducial field.

As in Lin et al. (1996) and Tucker et al. (1997), we make use of two different LCRS luminosity functions. The first version is the standard LCRS luminosity function; it best describes the data from the 112-fiber fields and the Northern Galactic Cap 50-fiber fields. Since these data compose $\sim 90\%$ of the full LCRS sample, it is this version of the luminosity function which we use for our fiducial field. The Schechter parameters for this luminosity function are as follows:

$$\alpha = -0.70, M^* = -20.29 + 5\log h, \phi^* = 0.019h^3 \ {\rm Mpc}^{-3} \tag{A3}$$

(M^* is the absolute magnitude equivalent of L^*).

The measured luminosity function for the 50-fiber Southern Galactic Cap data differs significantly from that of the other LCRS data (Lin et al. 1996). The reason behind this difference has never been fully resolved, but it is thought to be the effect of subtle selection problems in the very early LCRS data. We use the following values to describe the luminosity function of these Southern 50-fiber data:

$$\alpha = -0.74, M^* = -20.55 + 5\log h, \phi^* = 0.016h^3 \ {\rm Mpc}^{-3}. \tag{A4}$$

[Note: Both Equations A1 and A2 are actually simplified forms of the integral found in the group-finding code. The integral in the code also includes effects due to apparent magnitude and surface brightness incompleteness and due to central surface brightness selection; furthermore, in the code, this integral is convolved with a gaussian flux error of $\sigma = 0.1$ mag. For a detailed discussion of these additional selection effects, see § 3.2 of Lin et al. 1996.]

B. Calculating $L_{\rm tot}$ and $\sigma_{L_{\rm tot}}$ for Las Campanas Loose Groups

To correct for selection effects, $L_{\rm tot}$ is calculated by means of the following equation:

$$L_{\rm tot} = \sum_{i=1}^{N_{\rm obs}} \mathcal{L}_i, \tag{B1}$$

where

$$\mathcal{L}_i \equiv \left(\frac{n_{\rm lum}^{\rm tot}}{n_{\rm lum}^{\rm exp}(f_i, D(z_i))} \right) \times L_i, \tag{B2}$$

where $N_{\rm obs}$ is the number of *observed* members in the group, L_i is the luminosity of group member i, $n_{\rm lum}^{\rm tot}$ is the *total* expected luminosity density of *all* galaxies in the local Universe, and $n_{\rm lum}^{\rm exp}(f_i, D(z_i))$ is the expected luminosity density for only those galaxies that would lie within the photometric boundaries of LCRS field f_i at a comoving distance $D(z_i)$.

To estimate $n_{\rm lum}^{\rm tot}$, we integrate the luminosity-weighted Schechter function over all luminosities ($0 \leq L \leq \infty$):

$$\begin{aligned} n_{\rm lum}^{\rm tot} &= \phi^* L^* \int_0^\infty \left(\frac{L}{L^*}\right)^{\alpha+1} e^{-L/L^*} d\left(\frac{L}{L^*}\right) \\ &= \phi^* L^* \Gamma(\alpha+2), \end{aligned} \tag{B3}$$

where ϕ^*, α, and L^* are the standard Schechter parameters, and where Γ is the complete gamma function from mathematics (Abramowitz & Stegun 1970).

We estimate $n_{\rm lum}^{\rm exp}(f_i, D(z_i))$ via

$$n_{\rm lum}^{\rm exp}(f_i, D(z_i)) = F(f_i) \times \phi^* L^* \int_{L_{\rm min}}^{L_{\rm max}} \left(\frac{L}{L^*}\right)^{\alpha+1} e^{-L/L^*} d\left(\frac{L}{L^*}\right). \tag{B4}$$

Similar to the cases of equations A1 and A2, equation B4 is just the luminosity-weighted Schechter function multiplied by a corrective factor $F(f_i)$ and integrated over the interval $L_{\rm min} \leq L \leq L_{\rm max}$. $L_{\rm min}$ and $L_{\rm max}$ are the extremal luminosities observable at redshift z_i under the given flux and luminosity limits imposed on field f_i; $F(f_i)$ is the field-to-field sampling fraction for field f_i. [Note: Equation B4 is actually a simplified form of the integral found in the group-finding code. The integral in the code also includes effects due to apparent magnitude and surface brightness incompleteness and due to central surface brightness selection; furthermore, in the code, this integral is convolved with a gaussian flux error of $\sigma = 0.1$ mag. For a detailed discussion of these additional selection effects, see § 3.2 of Lin et al. 1996.]

The rms error in $L_{\rm tot}$ is estimated by summing the individual contributions from the rms errors in $\mathcal{L}_i$ in quadrature, yielding

$$\sigma_{L_{\rm tot}} = N_{\rm obs}\sqrt{\frac{<\mathcal{L}_i^2> - <\mathcal{L}_i>^2}{N_{\rm obs}-1}}, \tag{B5}$$

where

$$<\mathcal{L}_i> = \frac{\sum_{i=1}^{N_{\rm obs}} \mathcal{L}_i}{N_{\rm obs}} \tag{B6}$$

and

$$<\mathcal{L}_i^2> = \frac{\sum_{i=1}^{N_{\rm obs}} \mathcal{L}_i^2}{N_{\rm obs}}. \tag{B7}$$

C. Estimating Abell Counts for Las Campanas Loose Groups

We wish to make a quantitative, unbiased estimate of the richnesses of the Las Campanas loose groups. A useful and historically motivated method is to calculate their Abell counts, C. C was defined by Abell (1958) to be the number of galaxies, corrected for background contamination, in the magnitude interval m_3 to m_3+2 that lie within a 1.7 arcmin/z ($\approx 1.5\ h^{-1}$ Mpc) projected separation of a cluster's center; the magnitude m_3 is the magnitude of the third brightest cluster member. Due to the sampling characteristics and the relatively small range of apparent magnitudes within the LCRS, we cannot use Abell's definition directly. We must take a more circuitous path, via the use of the Schechter function for groups and clusters of galaxies.

For simplicity, consider a group which lies entirely within a single field. In this case, $n_{1.5}^{\rm obs}$, the observed number of galaxies within a 1.5 h^{-1} Mpc projected separation of a group's barycenter, should fit the relation

$$n_{1.5}^{\rm obs} = F(f_i) \times n_{1.5}^{*} \int_{L_{\rm min}}^{L_{\rm max}} \left(\frac{L}{L^*}\right)^{\alpha} e^{-L/L^*} d\left(\frac{L}{L^*}\right), \tag{C1}$$

which is just the integral of the Schechter function over the luminosity range $L_{\rm min} \le L \le L_{\rm max}$. As in Appendix B, $L_{\rm min}$ and $L_{\rm max}$ are the extremal luminosities observable at redshift z_i under the given flux and luminosity limits imposed on field f_i, and $F(f_i)$ is the field-to-field sampling fraction for field f_i. Here, $n_{1.5}^{*}$ is a normalization factor for galaxy number counts within a projected radius of 1.5 h^{-1} Mpc of a given group's barycenter; it is a counterpart to ϕ^*, which is used for the field galaxy luminosity function. The value for $n_{1.5}^{*}$ is itself a measure of richness; the richer the group or cluster, the higher the value of $n_{1.5}^{*}$ (assuming constant α and L^*). We will use $n_{1.5}^{*}$ to make an estimate of group Abell richness. Observationally, we can calculate a value for $n_{1.5}^{\rm obs}$ in equation C1 by subtracting off the estimated number of interlopers ($n_{\rm I}$; equation 14) from the total number of observed galaxies in a group within 1.5 h^{-1} Mpc of the group's barycenter ($N_{\rm obs}^{1.5}$),

$$n_{1.5}^{\rm obs} = \sum_{1}^{N_{\rm obs}^{1.5}} [1 - n_{\rm I}(f_i, cz_i)] \tag{C2}$$

Then, placing this result into equation C1,

$$n_{1.5}^{*} = \frac{n_{1.5}^{\rm obs}}{F(f_i)\int_{L_{\rm min}}^{L_{\rm max}} \left(\frac{L}{L^*}\right)^{\alpha} e^{-L/L^*} d\left(\frac{L}{L^*}\right)}. \tag{C3}$$

Since the LCRS is a $\sim$ 75%-sampled redshift catalogue with both bright and faint apparent magnitude cutoffs, it is quite possible that the third brightest group member may not be in the LCRS spectroscopic sample. Therefore, an estimate for the absolute magnitude of the third brightest group member must be computed. We can do this by integrating the group's luminosity function,

$$\begin{aligned} n_{\rm e}(\geq L) &= n_{1.5}^{*}\int_{L}^{\infty} \left(\frac{L}{L^*}\right)^{\alpha} e^{-L/L^*} d\left(\frac{L}{L^*}\right) \\ &= n_{1.5}^{*}\Gamma(\alpha+1, L/L^*), \end{aligned} \tag{C4}$$

where $\Gamma(\alpha+1, L/L^*)$ is the incomplete gamma function (Abramowitz & Stegun 1970), and solving the equation

$$n_{\rm e}(\geq L(m_3)) = 3 = n_{1.5}^{*}\Gamma(\alpha+1, L(m_3)/L^*) \tag{C5}$$

numerically for the luminosity of the third brightest cluster member, $L(m_3)$. Finally, taking our estimate of $n_{1.5}^{*}$ from equation C3 and our estimate of $L(m_3)$ from equation C5, we can calculate the group's Abell Richness, which we will call $C_{\rm grp}$,

$$C_{\rm grp} = n_{1.5}^{*}\int_{L(m_3)}^{L(m_3+2)} \left(\frac{L}{L^*}\right)^{\alpha} e^{-L/L^*} d\left(\frac{L}{L^*}\right), \tag{C6}$$

where $L(m_3+2)$ is the luminosity associated with the apparent magnitude m_3+2 at the redshift of the group in question.

A further complication exists in that the linking radius employed in the "friends-of-friends" percolation algorithm is only ~ 1 h^{-1} Mpc at the fiducial redshift $z_{\rm fid}$; for some tightly configured groups containing only a few observed members, the full Abell radius of 1.5 h^{-1} Mpc (projected) may not be completely searched, resulting in underestimates of the Abell counts C. Since most LCRS groups are not very tightly configured (consider the mean pairwise separations, $R_{\rm p}$), this is not likely to be a significant effect for the catalogue as a whole. In a similar case, APM clusters, which number counts only within a projected radius of 0.75 h^{-1} Mpc from the cluster center, have been shown to underestimate their Abell counts typically by only $\sim 20\%$ or less (Bahcall & West 1992). The LCRS percolation algorithm, with its relatively large linking parameter $D_{\rm L}$ (typically $\gtrsim 1 h^{-1}$ Mpc), should perform much better than do the APM counts.

When compared with actual Abell clusters within the LCRS volume, we find the following relation between the LCRS group counts estimate, $C_{\rm grp}$, and the revised Abell cluster values given by ACO, $C_{\rm ACO}$:

$$C_{\rm grp} \quad \sim \quad 0.19 C_{\rm ACO} + 12$$

(eq. [41]). We discuss this relation in more detail in § 6.

REFERENCES

Abell, G. O. 1958, ApJS, 3, 211

Abell, G. O., Corwin, H. G., & Olowin, R. P. 1989, ApJS, 70, 1 (ACO)

Abramowitz, M., & Stegun, I. A. 1970, Handbook of Mathematical Functions with Formulas, Graphs, and Mathematical Tables (Washington, DC: US Government Printing Office)

Allam, S. S., Tucker, D. L., Lin, H., Hashimoto, Y. 1999, ApJ, 522, L89

Allington-Smith, J. R., Ellis, R. S., Zirbel, E. L., & Oemler, A. 1993, ApJ, 404, 521

Bahcall, N., & West, M. 1992, ApJ, 392, 419

Bevington, P. R. 1969, Data Reduction and Error Analysis for the Physical Sciences (New York: McGraw-Hill, Inc.)

Binney, J., & Tremaine, S. 1987, Galactic Dynamics (Princeton: Princeton Univ. Press)

Deming, W. E. 1950, Some Theory of Sampling (New York: Dover)

de Lapparent, V., Geller, M. J., & Huchra, J. P. 1988, ApJ, 332, 44

de Vaucouleurs, G. 1975, in Galaxies and the Universe, ed. A. Sandage, M. Sandage, & J. Kristian (Chicago: Univ. Chicago Press), 557

Diaferio, A., Ramella, M., Geller, M. J., & Ferrari, A. 1993, AJ, 105, 2035

Geller, M. J., & Huchra, J. P. 1983, ApJS, 52, 61 (GH83)

Giovanelli, R., & Haynes, M. P. 1993, AJ, 105, 1271

Gott, J. R., III, & Turner, E. L. 1977, ApJ, 213, 309

Harrison, E. R. 1974, ApJ, 191, L51

Hashimoto, Y., & Oemler, A. 1998, astro-ph/9807275

Hashimoto, Y., Oemler, A., Lin, H., & Tucker, D. L. 1998, ApJ, 499, 589

Holmberg, E. 1969, Ark. Astr., 5, 305

Huchra, J. P., & Geller, M. J. 1982, ApJ, 257, 423 (HG82)

Huchra, J. P., Geller, M. J., de Lapparent, V., & Corwin, H. G. 1990, ApJS, 72, 433

Huchra, J. P., Geller, M. J., & Corwin, H. G. 1995, ApJS, 99, 391

Lin, H., Kirshner, R. P., Shectman, S. A., Landy, S. D., Oemler, A., Tucker, D. L., & Schechter, P. L. 1996, ApJ, 464, 60

Lineweaver, C. H., Tenorio, L., Smoot, G. F., Keegstra, P., Banday, A. J., & Lubin, P. 1996, ApJ, 470, 38

Maia, M. A. G., da Costa, L. N., & Latham, D. W. 1989, ApJS, 69, 809 (MdCL89)

Moore, B., Frenk, C. S., & White, S. D. M. 1993, MNRAS, 261, 827 (MFW93)

Nolthenius, R., & White, S. D. M. 1987, MNRAS, 225, 505 (NW87)

Nolthenius, R. 1993, ApJS, 85, 1 (N93)

Oemler, A. 1988, in The Minnesota Lectures on Clusters of Galaxies and Large-Scale Structure, ASP Conf. Ser., Vol. 5, ed. J. M. Dickey (San Francisco: ASP), 19

Oemler, A. 1992, in Clusters and Superclusters of Galaxies, NATO ASI Series C, Vol. 266, ed. A. C. Fabian (Dordrecht: Kluwer), 29

Pinsonnealt, M., private communication

Postman, M., & Geller, M. J. 1984, ApJ, 281, 95

Ramella, M., Geller, M. J., & Huchra, J. P. 1989, ApJ, 344, 57 (RGH89)

Ramella, M., Pisani, A., & Geller, M. J. 1997, AJ, 113, 483 (RGP97)

Ramella, M., Zamorani, G., Zucca, E., et al. 1999, A&A, 342, 1 (RZZ99)

Schechter, P. 1976, ApJ, 203, 297

Shectman, S. A., Landy, S. D., Oemler, A., Tucker, D. L., Lin, H., Kirshner, R. P., & Schechter, P. L. 1996, ApJ, 470, 172

Trasarti-Battistoni, R. 1998, A&AS, 130, 341 (TB98)

Tucker, D. L. 1994, Ph.D. dissertation, Yale University (T94)

Tucker, D. L., Oemler, A, Kirshner, R. P., Lin, H., Shectman, S. A., Landy, S. D., Schechter, P. L., Müller, V., Gottlöber, S., & Einasto, J. 1997, MNRAS, 285, L5

Turner, E. L., & Gott, J. R. 1976, ApJS, 32, 409

Vettolani, G., Zucca, E., Zamorani, G., et al. 1997, A&A, 325, 954

Wegner, G., Haynes, M. P., & Giovanelli, R. 1993, AJ, 105, 1251

Whitmore, B. C., Gilmore, D. M., & Jones, C. 1993, ApJ, 407, 489

Zabludoff, A. I., Geller, M. J., Huchra, J. P., Ramella, M. 1993, AJ, 106, 1301

Zabludoff, A. I., Zaritsky, D., Lin, H., Tucker, D., Hashimoto, Y., Shectman, S. A., Oemler, A., & Kirshner, R. P. 1996, ApJ, 466, 104

This preprint was prepared with the AAS LaTeX macros v4.0.

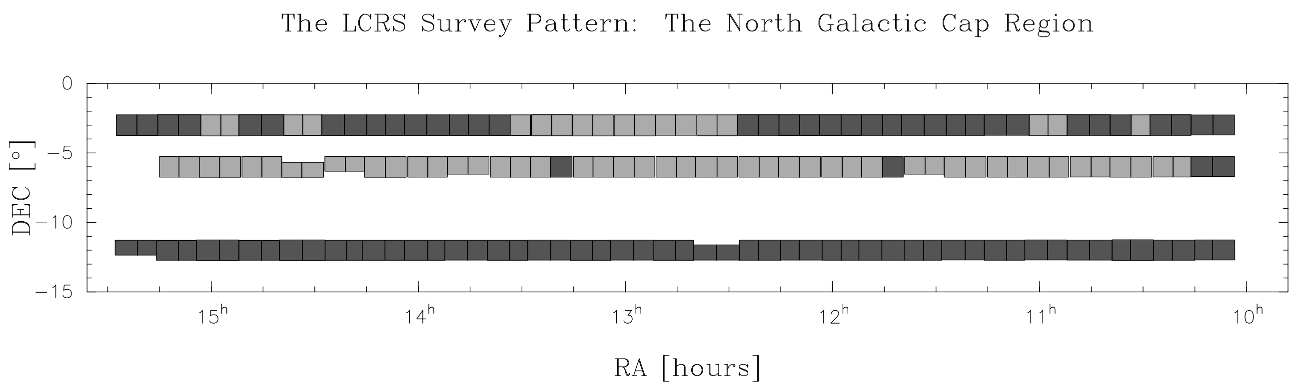

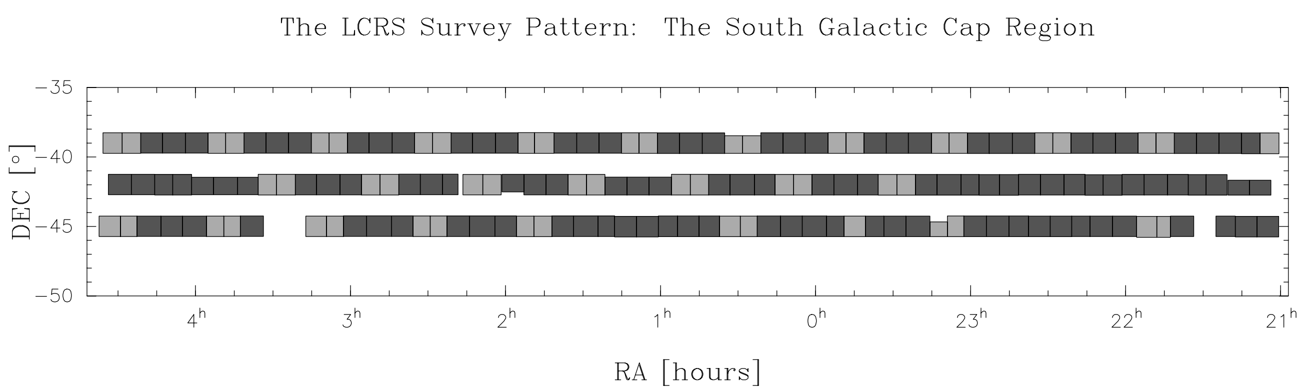

Fig. 1.— The LCRS survey pattern for the Northern (top) and the Southern (bottom) Galactic Cap regions. Lightly shaded regions denote fields observed with the 50-fiber MOS and darkly shaded regions fields observed with the 112-fiber MOS. Declination and right ascension coordinates are equinox 1950.0

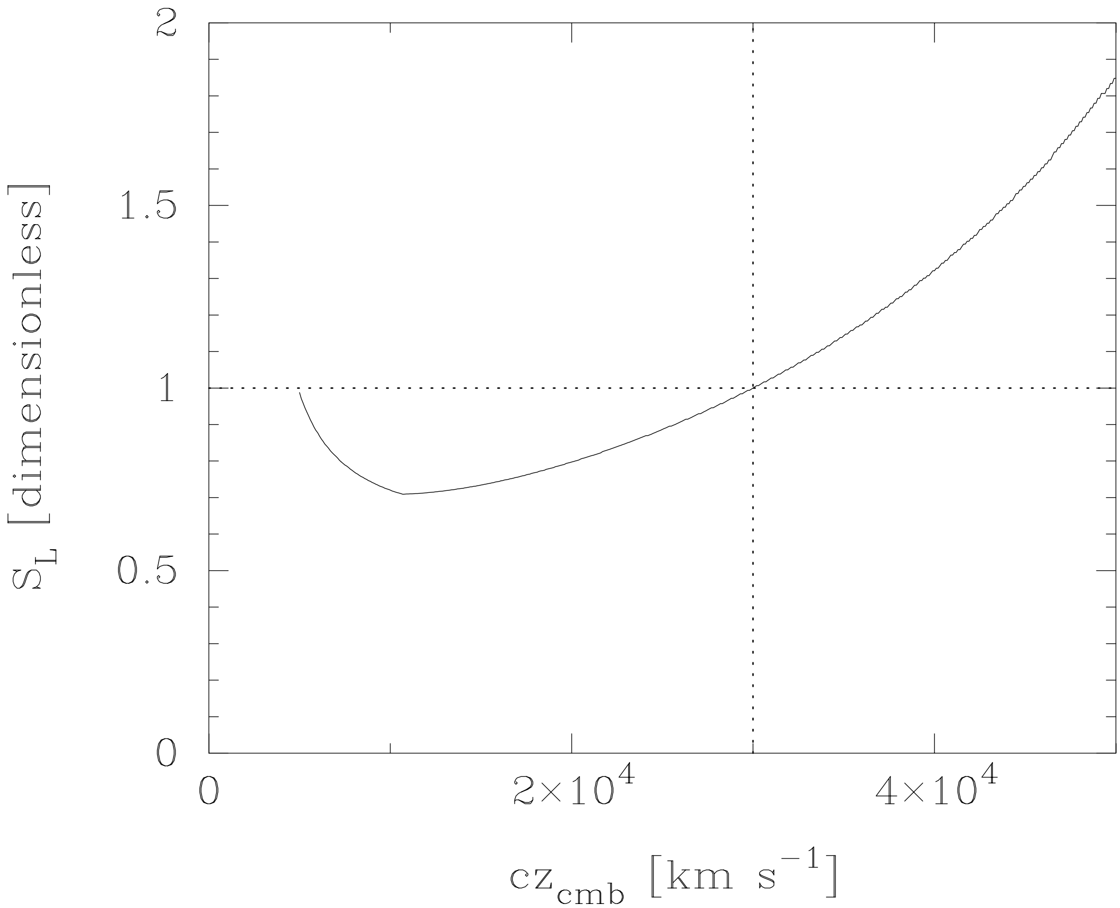

Fig. 2.— Variation of the linking scale S_{L} with velocity for the fiducial field ($15.0 \leq R < 17.7$, 100% sampling), assuming $\alpha = -0.70$, $M^{*} = -20.29+5\log h$, and $\phi^{*} = 0.019h^{3}$ Mpc^{-3}. The dotted lines indicate the locus of $S_{\mathrm{L}} = 1$ and $cz_{\mathrm{cmb}} = 30,000$ km s^{-1} (the fiducial velocity).

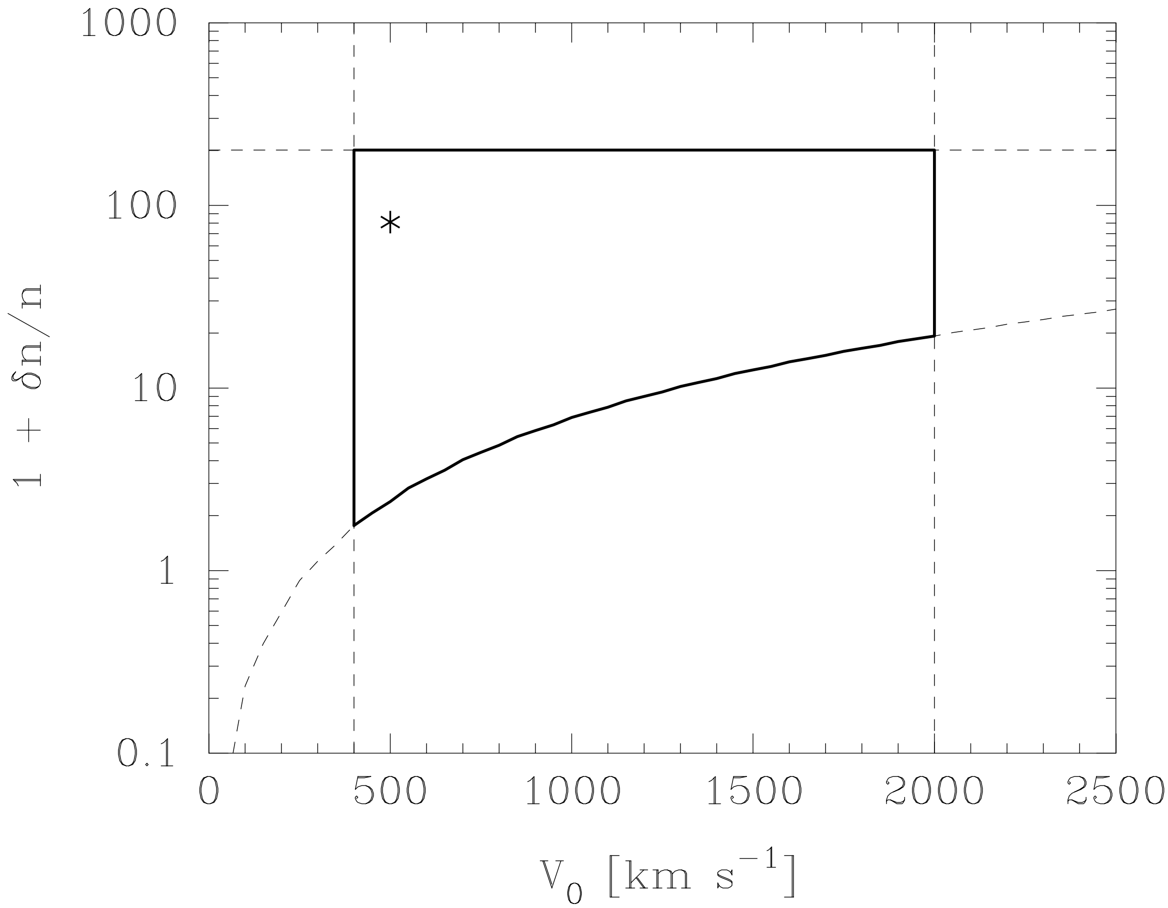

Fig. 3.— Group selection parameters. The region of reasonable search parameter values is bound in solid (see text for details). The asterisk indicates the final choice used in extracting the LCRS group catalogue: $\delta n/n = 80$ ($\Longleftrightarrow D_0 = 0.715\ h^{-1}$ Mpc) and $V_0 = 500$ km s^{-1}.

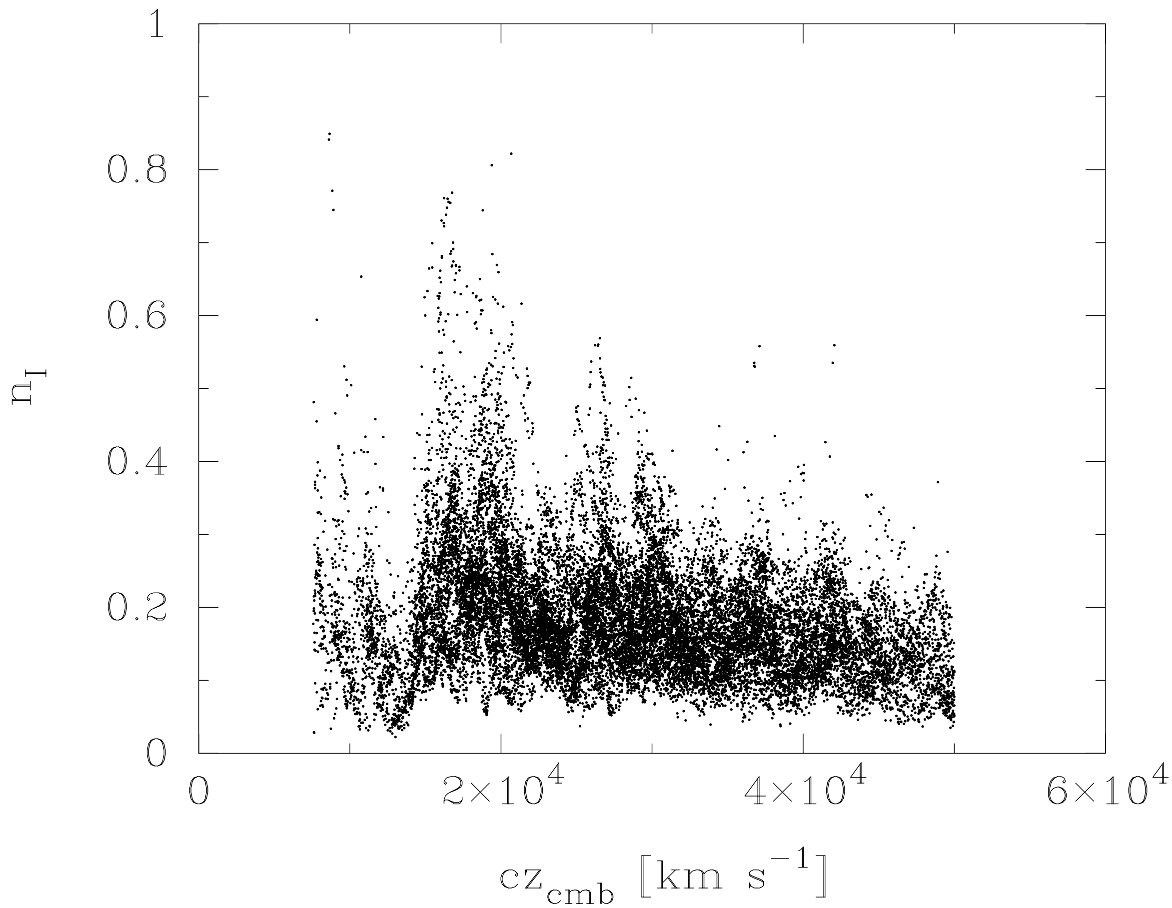

Fig. 4.— The number of interlopers per galaxy, n_I, at the redshift of each galaxy in the LCRS (assuming the final values for $\delta n/n$ (D_0) and V_0). The median n_I is 0.17 interlopers per galaxy.

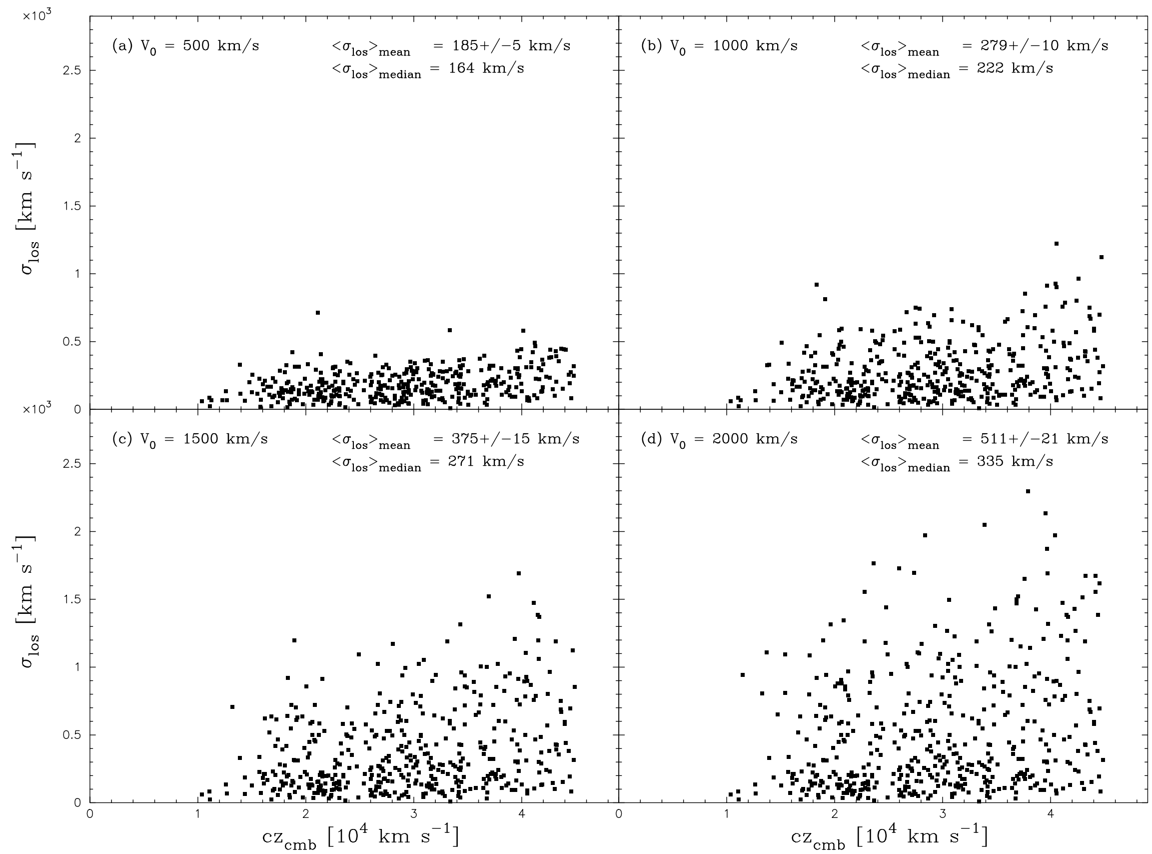

Fig. 5.— Group line-of-sight velocity dispersions vs. redshift for $\delta n/n = 80$ and (a) $V_0 = 500$ km s^{-1} (b) $V_0 = 1000$ km s^{-1}, (c) $V_0 = 1500$ km s^{-1}, and (d) $V_0 = 2000$ km s^{-1}. (N.B.: Only groups meeting the requirements of a clean sample — i.e., groups with $\sigma_{\rm los} > 0$ km s^{-1}, with barycenters $> 2R_{\rm p}$ from a slice edge, with crossing times < a Hubble time, and with no galaxies with a mock redshift — were included in these plots; for a more in-depth discussion of the requirements of a clean sample, see § 4.)

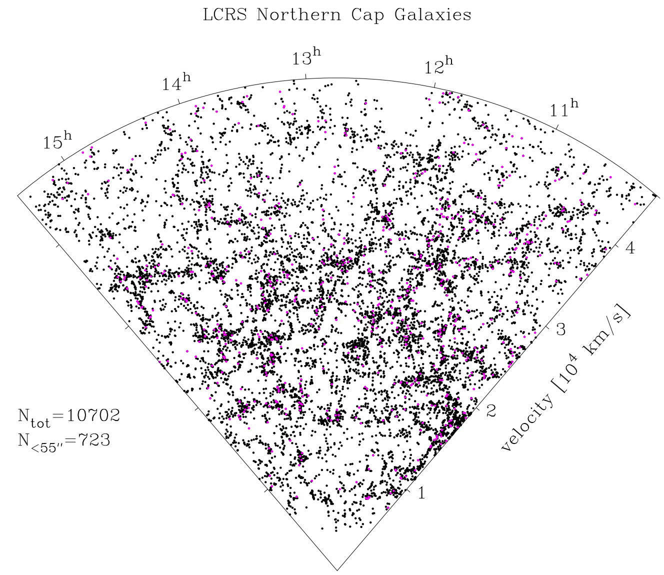

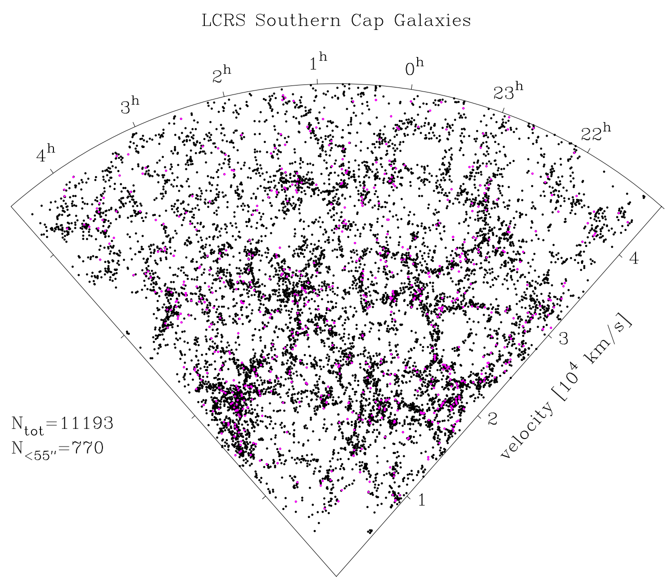

Fig. 6.— The distribution of galaxies in the LCRS Northern (top) and Southern (bottom) Galactics out to $cz = 46,000$ km s^{-1} (to include group members beyond the group catalogue $cz = 45,000$ km s^{-1} limit). Only those galaxies having luminosity $-22.5 \leq M_R - 5\log h < -17.5$ and lying within the LCRS official geometric and photometric boundaries are plotted. Red points are the 55-arcsec "orphans," plotted with their mock velocities. $N_{\rm tot}$ is the total number of galaxies plotted, 55-arcsec "orphans" included; $N_{<55''}$ refers to the number of 55-arcsec "orphans" plotted.

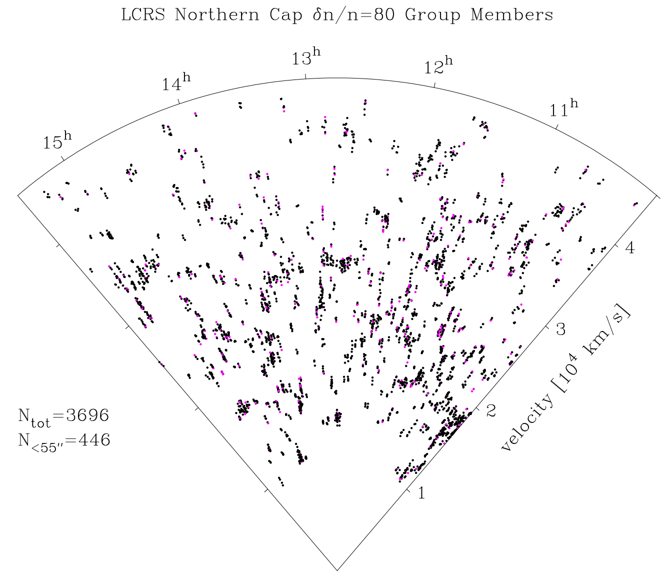

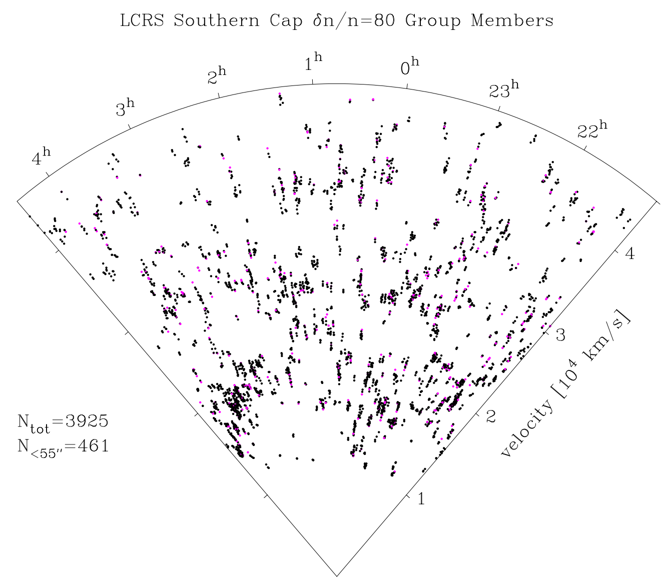

Fig. 7.— Same as Figure 6, but only galaxies in $\delta n/n = 80$ groups are plotted.

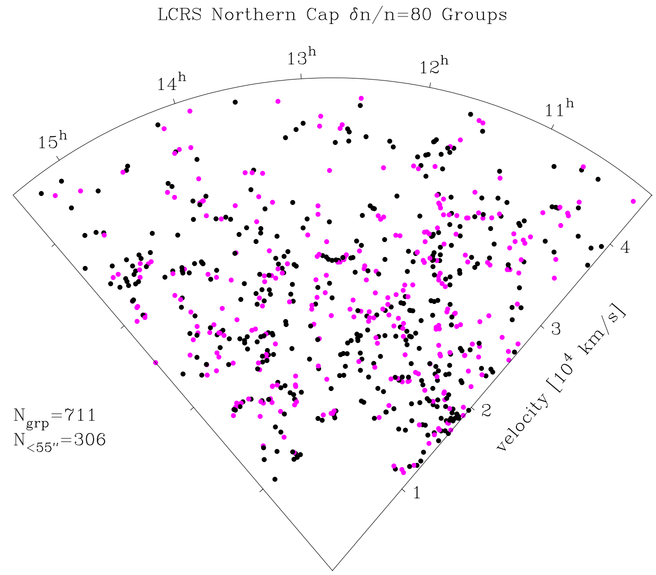

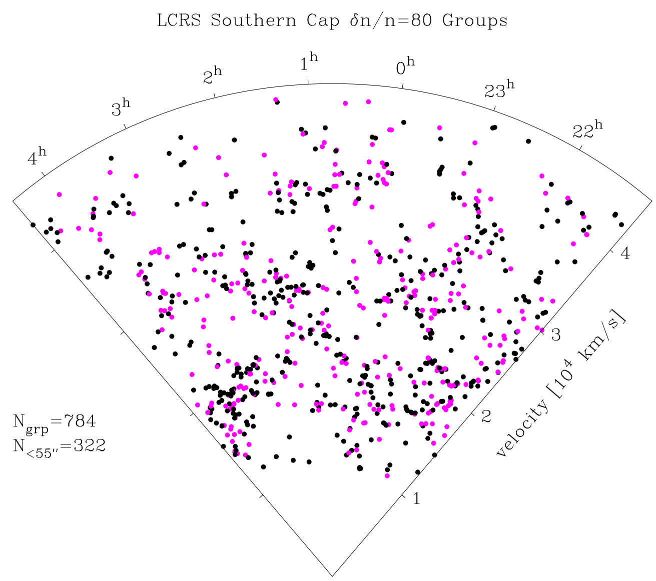

Fig. 8.— The distribution of $\delta n/n = 80$ groups in the LCRS Northern (top) and Southern (bottom) Galactic Caps. Red symbols indicate groups containing at least one 55-arcsec "orphan". $N_{\rm grp}$ refers to the total number of groups plotted, $N_{<55''}$ to the the number which contain 55-arcsec "orphans". (N.B.: The LCRS group catalogue extends from $cz = 10,000$ km s^{-1} to $cz = 45,000$ km s^{-1}; so the dearth of groups at $cz < 10,000$ km s^{-1} is not physical but merely the cutoff of the catalogue.)

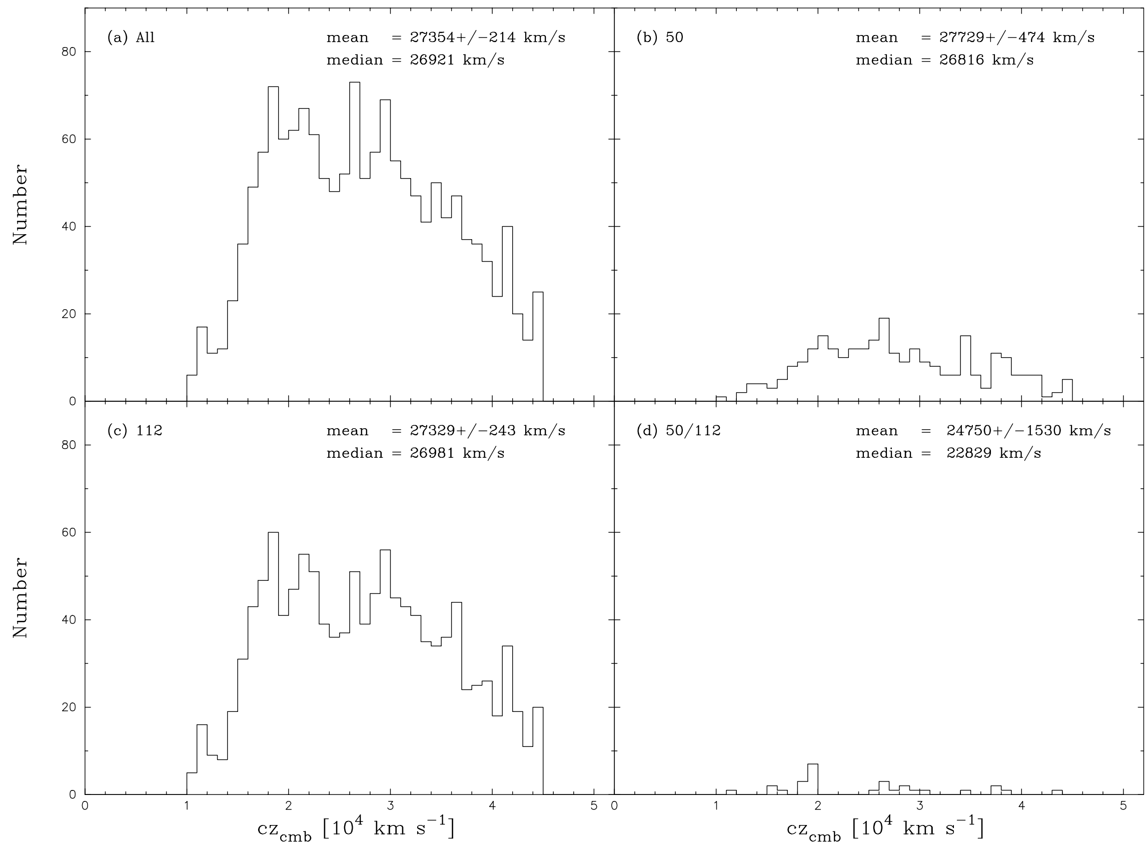

Fig. 9.— Distribution of group velocities from the full sample of 1495 groups: (a) all the groups, (b) just those groups in the 50-fiber fields, (c) just those groups in the 112-fiber fields, (d) just those groups which straddle a 50-/112-fiber field boundary.

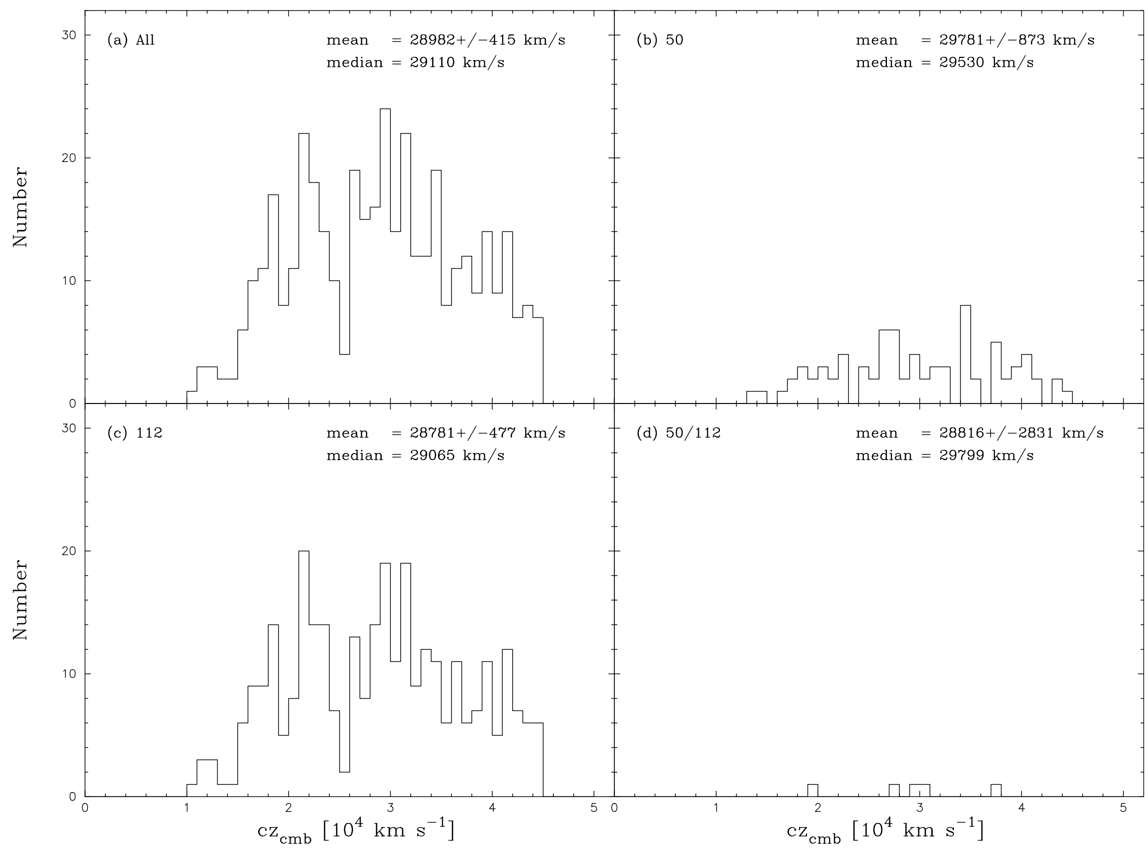

Fig. 10.— Distribution of group velocities from the clean sample of 394 groups: (a) – (d) are as in Figure 9.

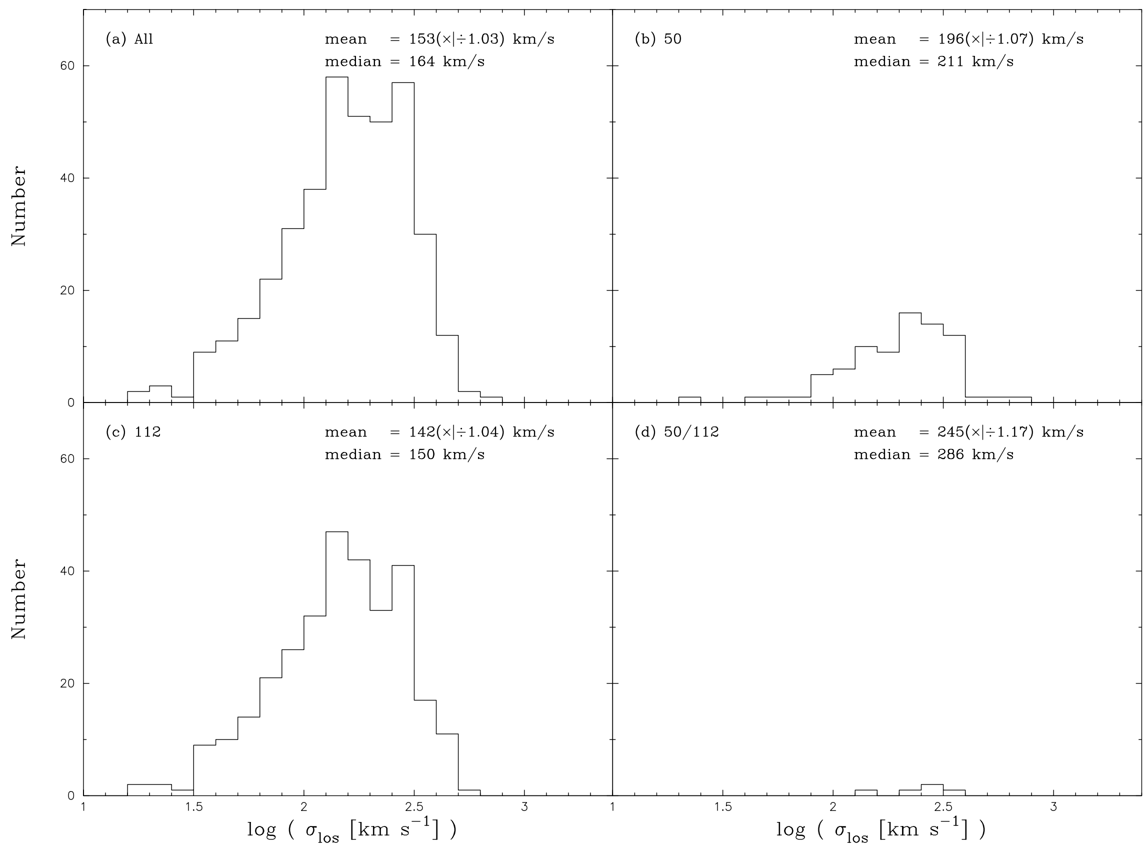

Fig. 11.— Distribution of line-of-sight velocity dispersions, $\sigma_{\rm los}$, for LCRS groups in the clean sample: (a) – (d) are as in Figure 9.

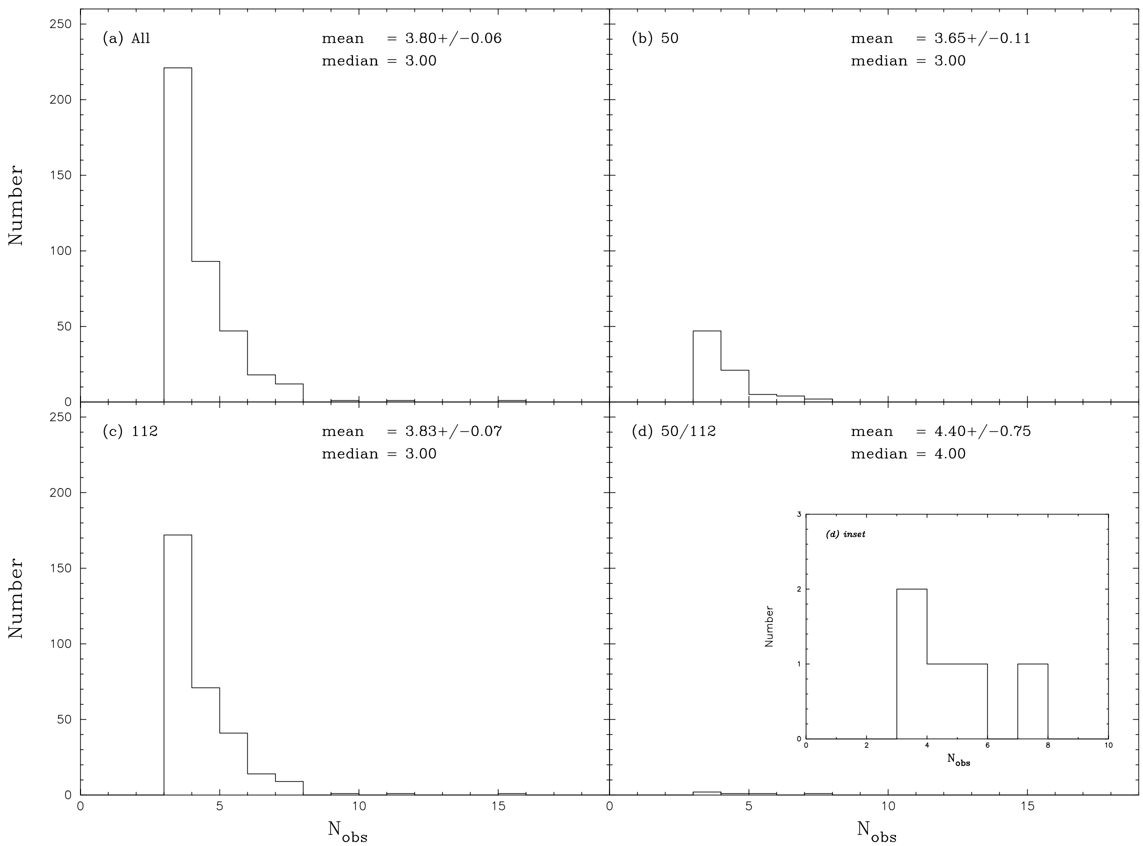

Fig. 12.— Distribution of the observed number of LCRS galaxies within a group, $N_{\rm obs}$, for the LCRS groups in the clean sample: (a) – (d) are as in Figure 9; inset of (d) is a merely a blow-up to aid the reader.

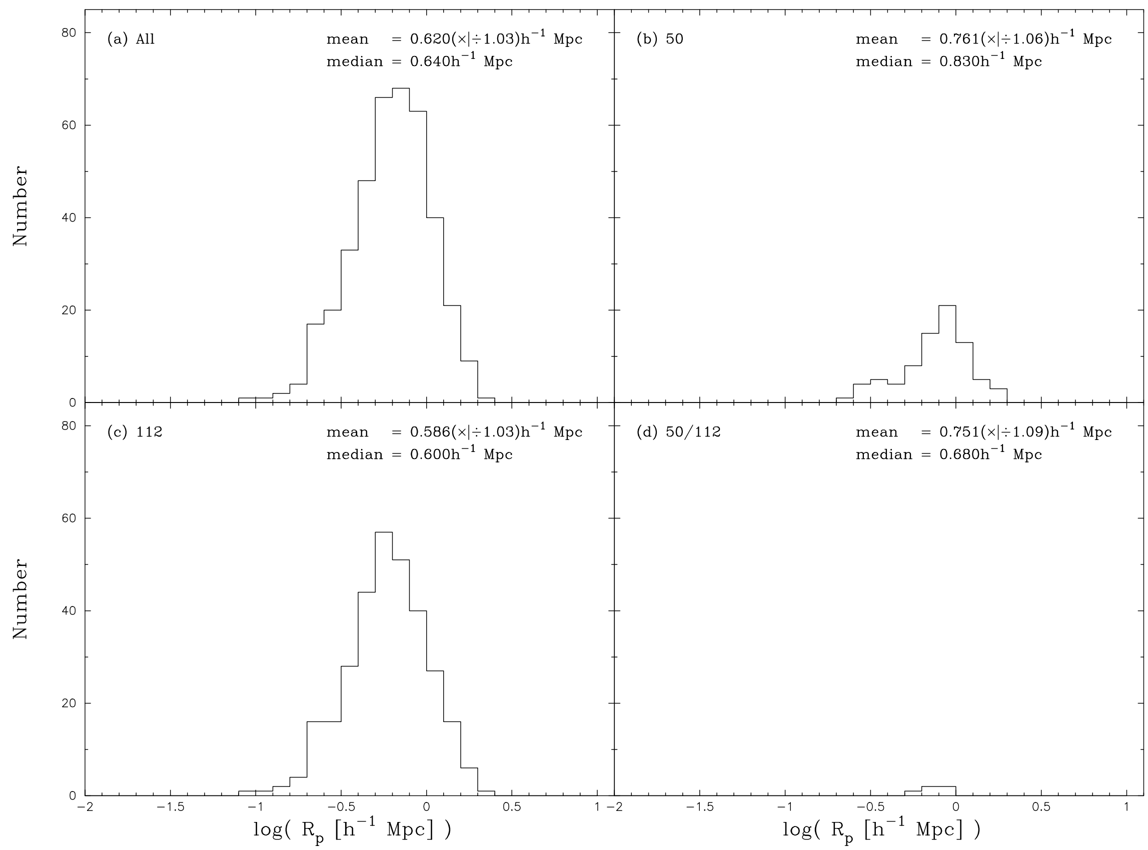

Fig. 13.— Distribution of mean pairwise separations, $R_{\rm p}$, for LCRS groups in the clean sample: (a) – (d) are as in Figure 9.

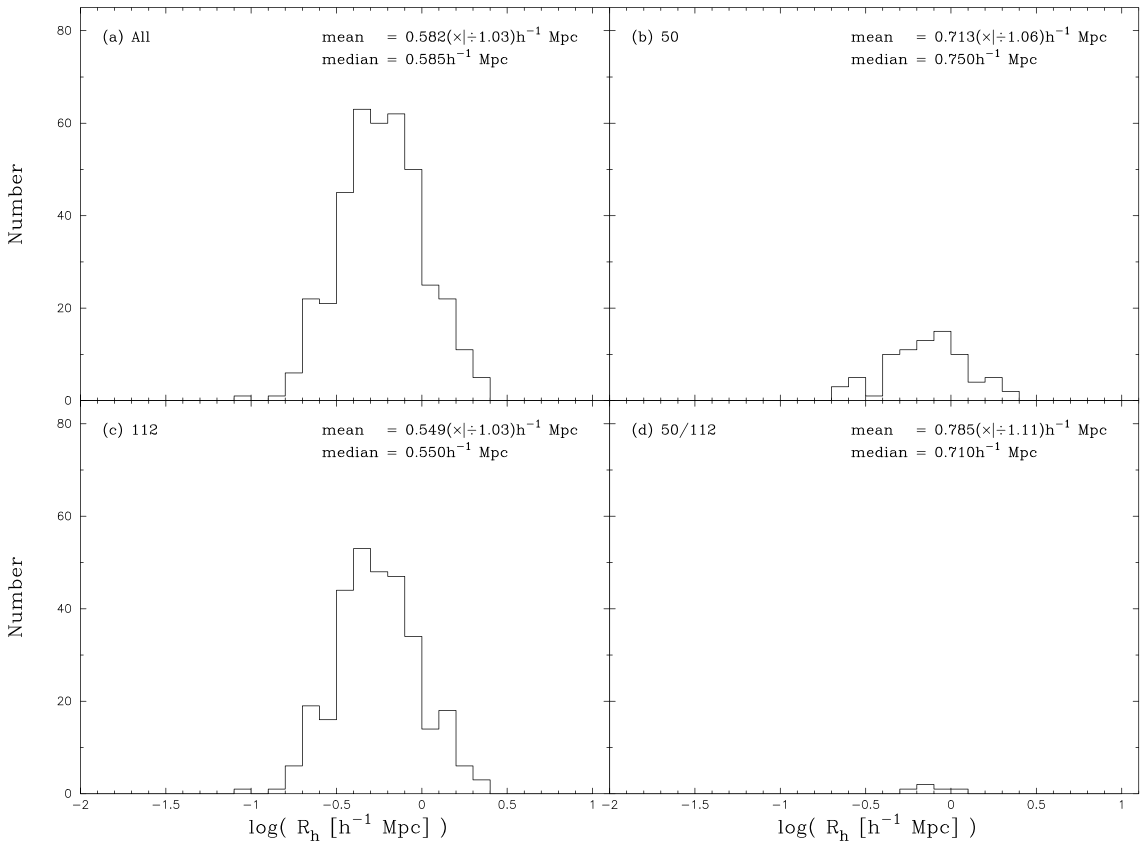

Fig. 14.— Distribution of harmonic radii, $R_{\rm h}$, for LCRS groups in the clean sample: (a) – (d) are as in Figure 9.

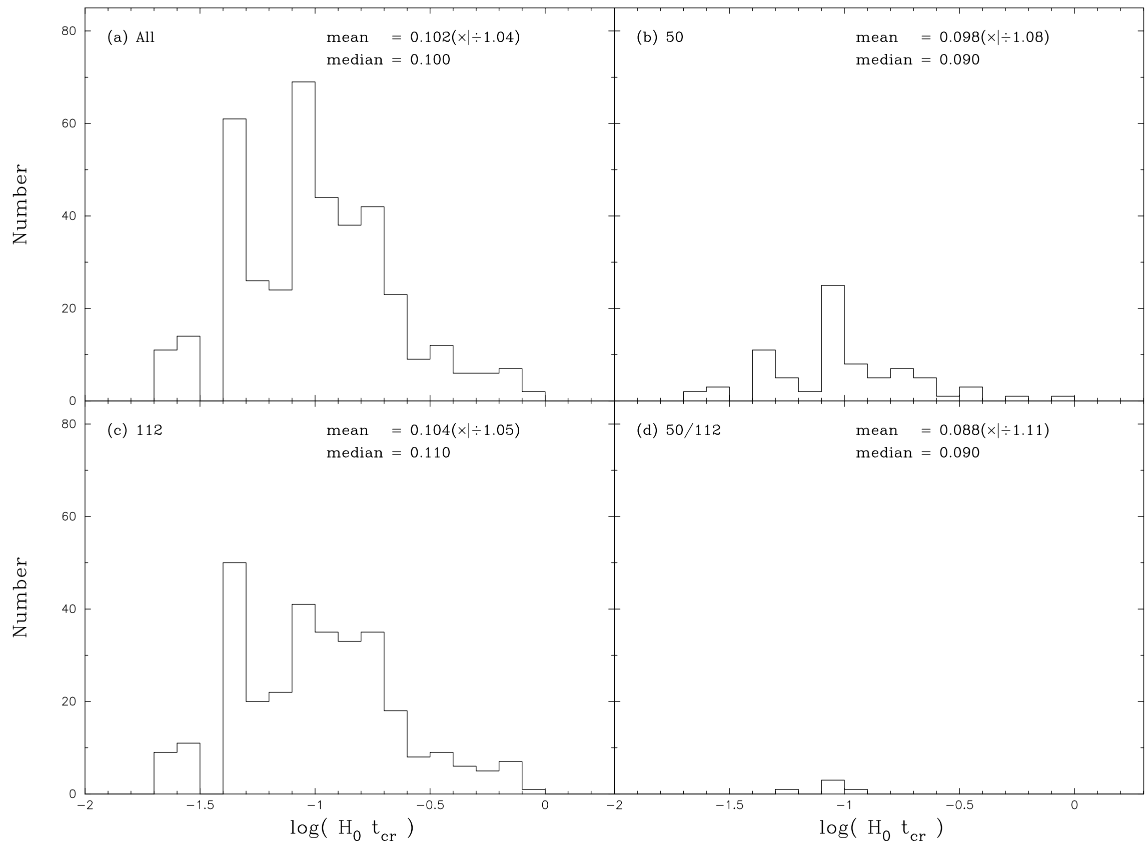

Fig. 15.— Distribution of virial crossing times, $t_{\rm cr}$, as a fraction of the Hubble time (H_0^{-1}), for LCRS groups in the clean sample: (a) – (d) are as in Figure 9. Following Gott & Turner (1977), groups with crossing times $t_{\rm cr} \lesssim 0.11 H_0^{-1}$ should have had enough time in the age of the Universe to virialize completely [but cf. Diaferio et al. (1993)].

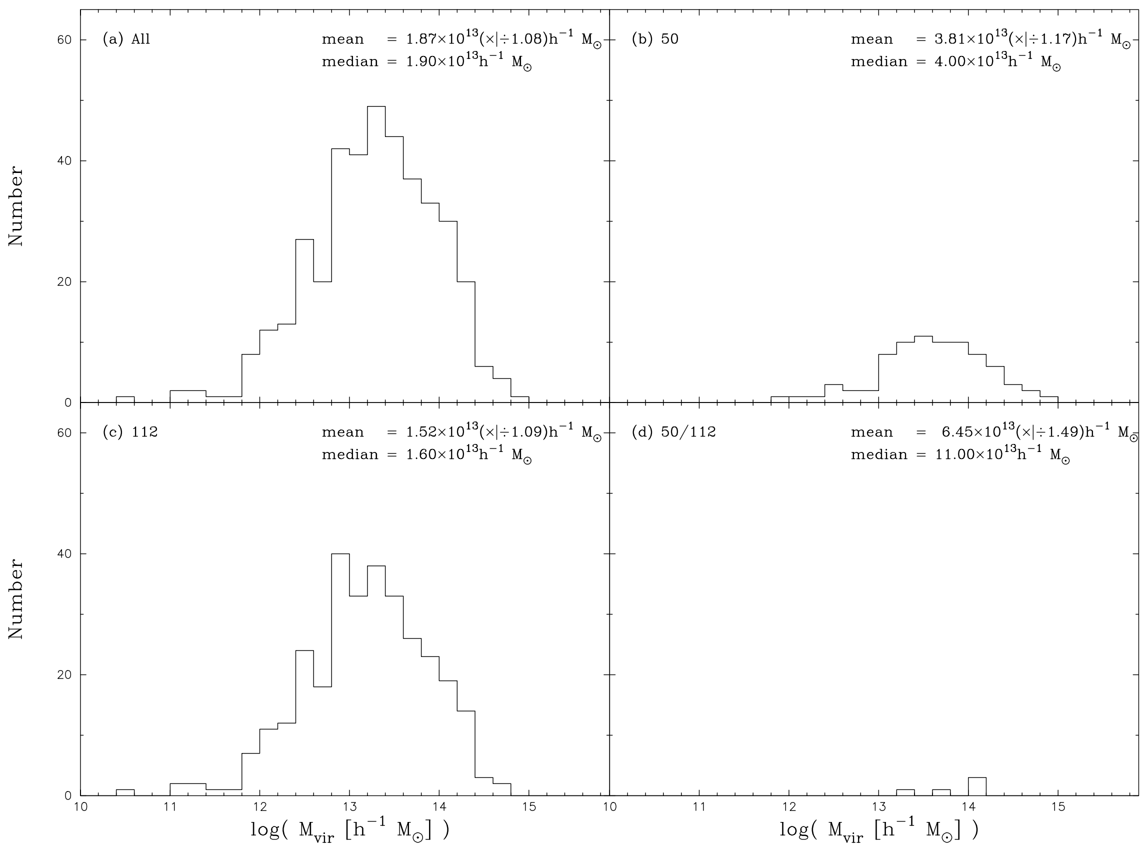

Fig. 16.— Distribution of virial masses, $M_{\rm vir}$, for LCRS groups in the clean sample: (a) – (d) are as in Figure 9.

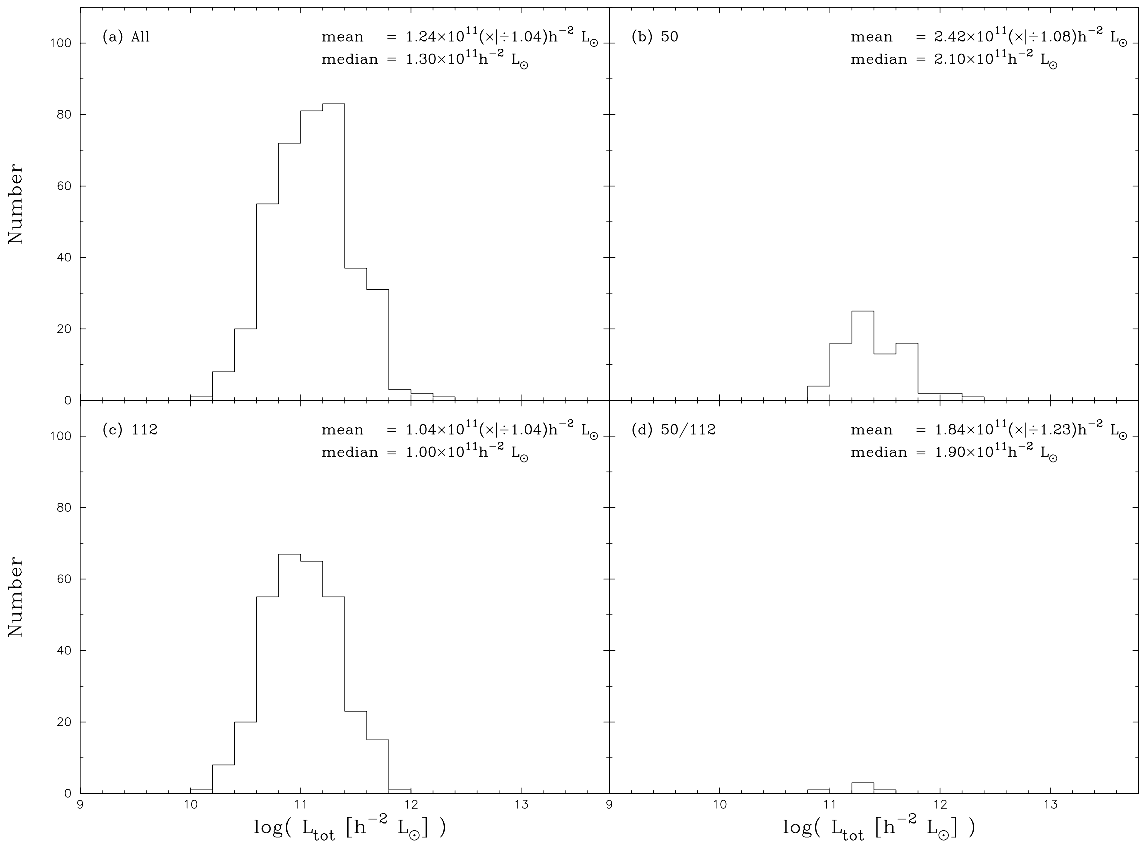

Fig. 17.— Distribution of estimated R-band total luminosities, $L_{\rm tot}$, for LCRS groups in the clean sample: (a) – (d) are as in Figure 9.

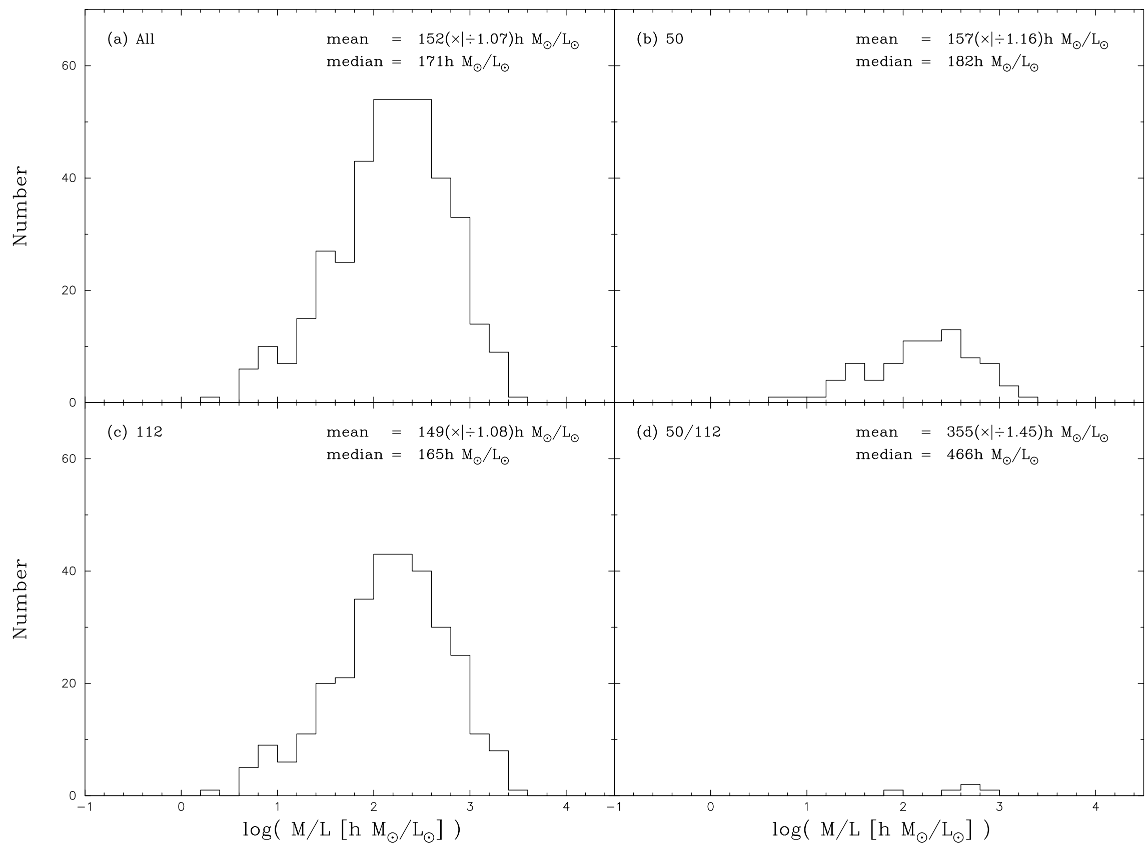

Fig. 18.— Distribution of estimated R-band mass-to-light ratios, M/L, for LCRS groups in the clean sample: (a) – (d) are as in Figure 9.

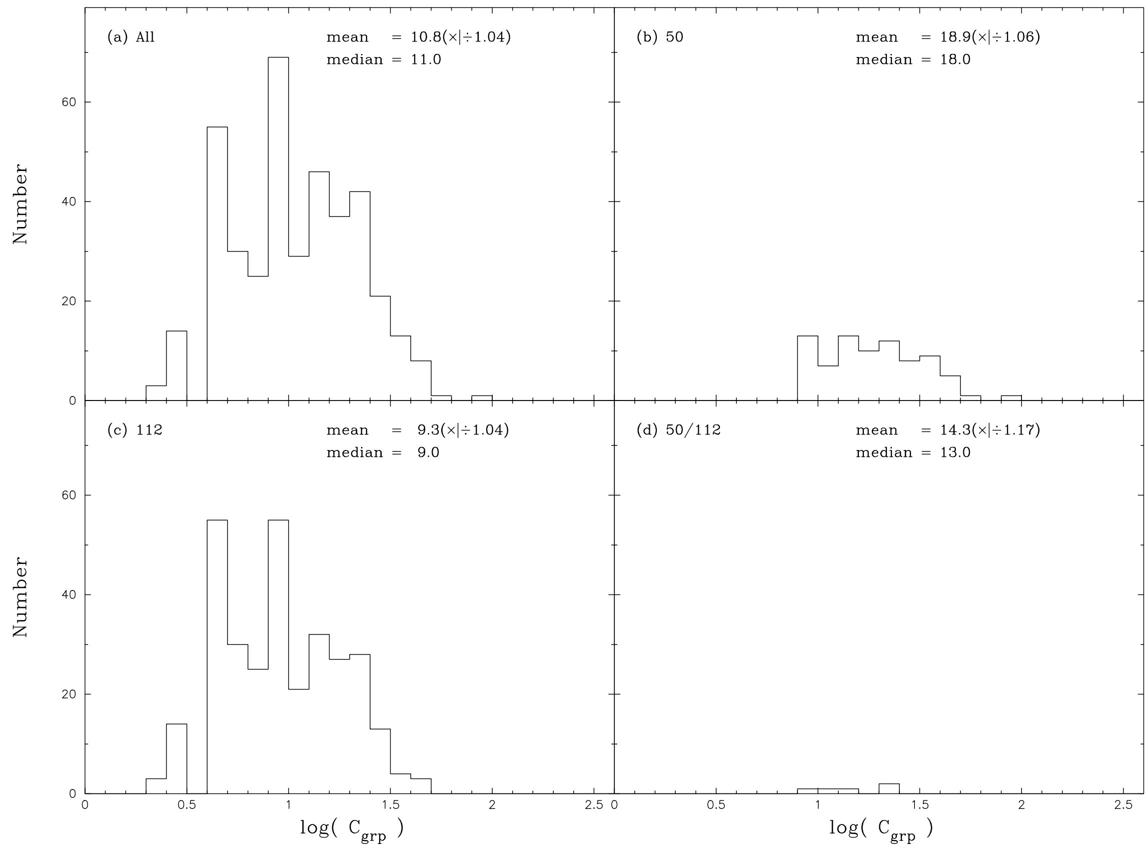

Fig. 19.— Distribution of Abell-like group counts (or richnesses), $C_{\rm grp}$, for LCRS groups in the clean sample: (a) – (d) are as in Figure 9.

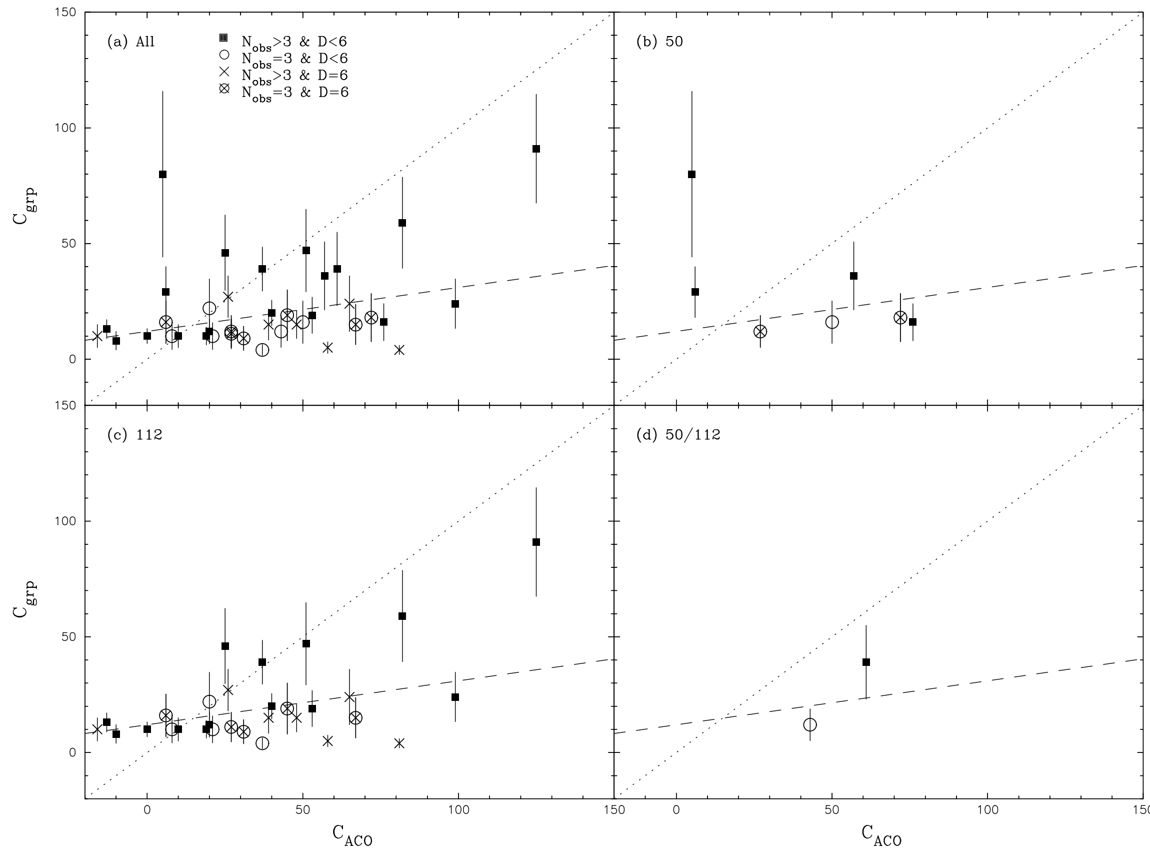

Fig. 20.— Group counts $C_{\rm grp}$ vs. Abell counts $C_{\rm ACO}$ for LCRS groups which are identified with an ACO cluster. The sample of LCRS groups used in the matchups was a superset of the clean sample (groups including galaxies with mock velocities were also included). *Filled squares* denote groups with more than 3 observed members matched with ACO clusters of Abell distance class $D < 6$; *open circles* denote groups with exactly 3 observed members matched with distance class $D < 6$ ACO clusters; $\times$*'s* denote groups with more than 3 observed members matched with distance class $D = 6$ ACO clusters; and $\times$*'ed circles* denote groups having exactly 3 observed members identified with distance class $D = 6$ ACO clusters. The *dotted line* represents the locus of $C_{\rm grp} = C_{\rm ACO}$; the *dashed line* represents the best-fit line, $C_{\rm grp} = 0.19C_{\rm ACO} + 12$, for $N_{\rm obs} > 3, D < 6$ matches. Plots (a) – (d) are as in Figure 9.

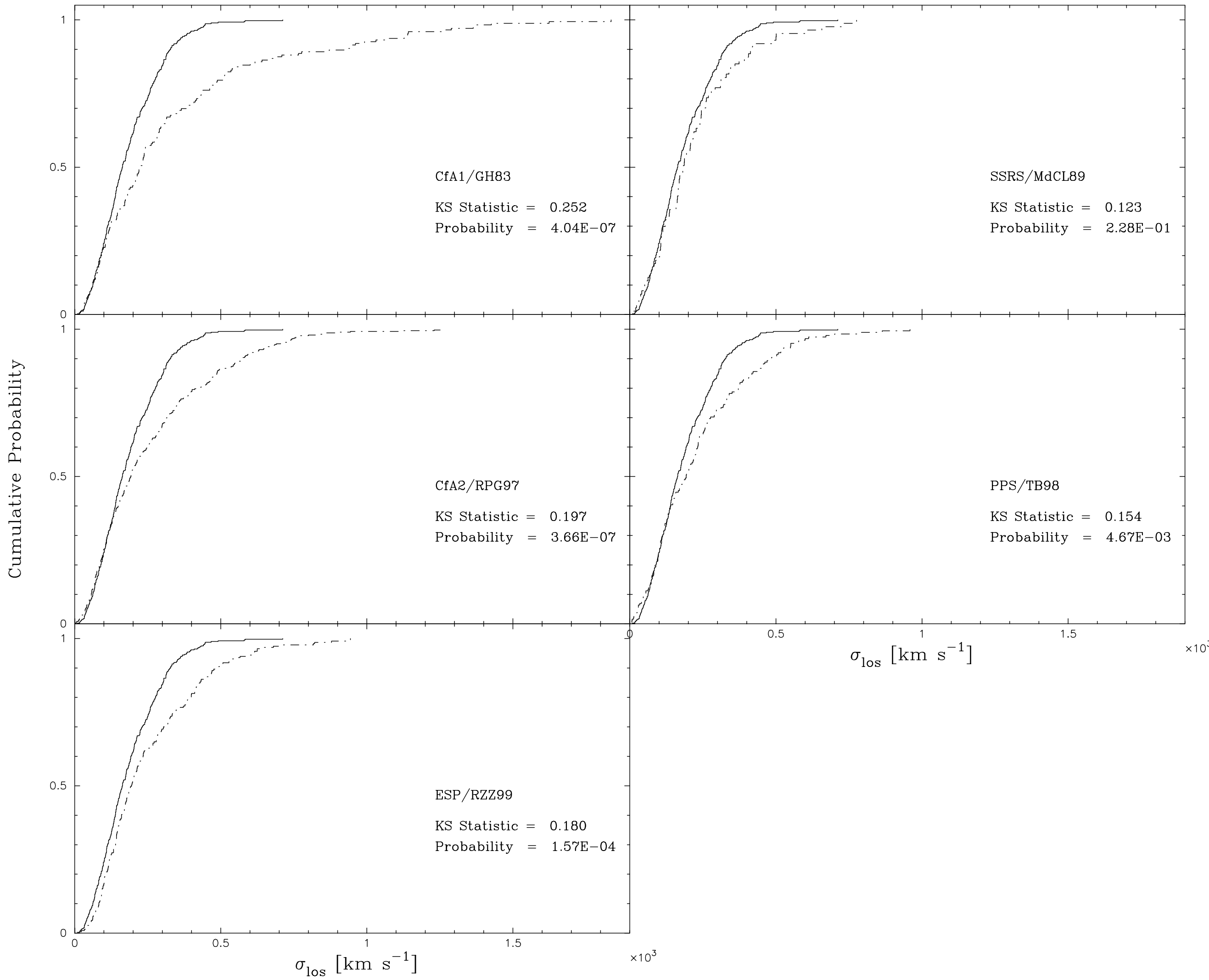

Fig. 21.— KS tests comparing the distribution of line-of-sight velocity dispersions from various group catalogues (*dot-dashed line*) against that from the full LCRS group catalogue (*solid line*).

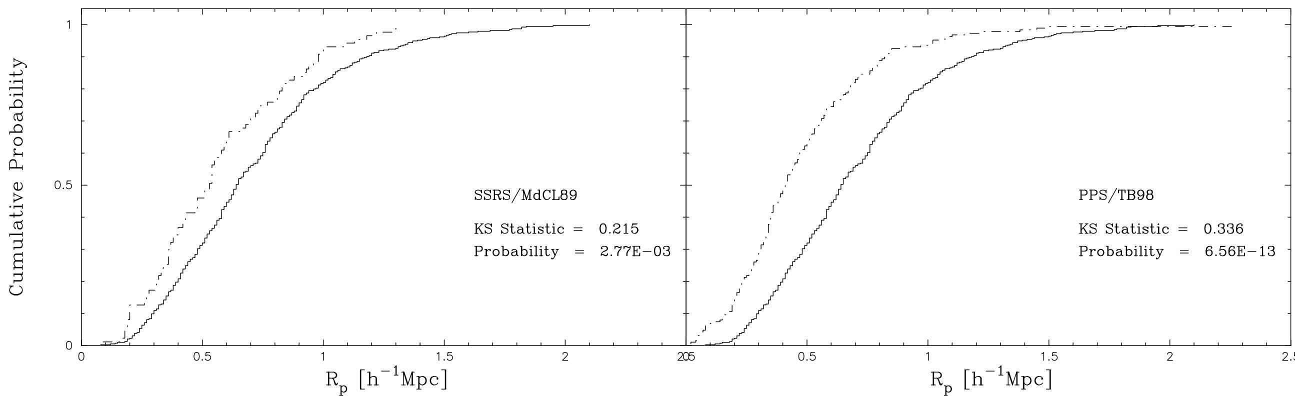

Fig. 22.— KS tests comparing the distribution of mean pairwise separations from various group catalogues (*dot-dashed line*) against that from the full LCRS group catalogue (*solid line*).

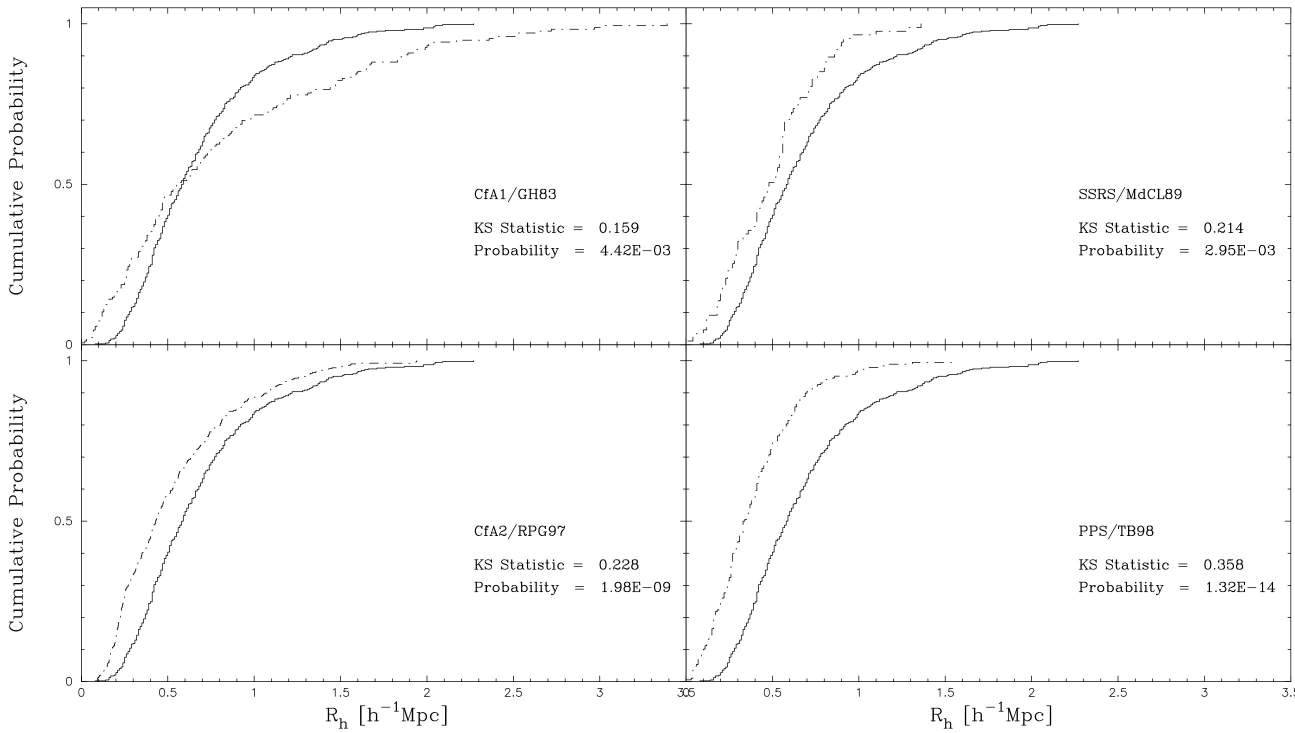

Fig. 23.— KS tests comparing the distribution of harmonic radii from various group catalogues (*dot-dashed line*) against that from the full LCRS group catalogue (*solid line*).

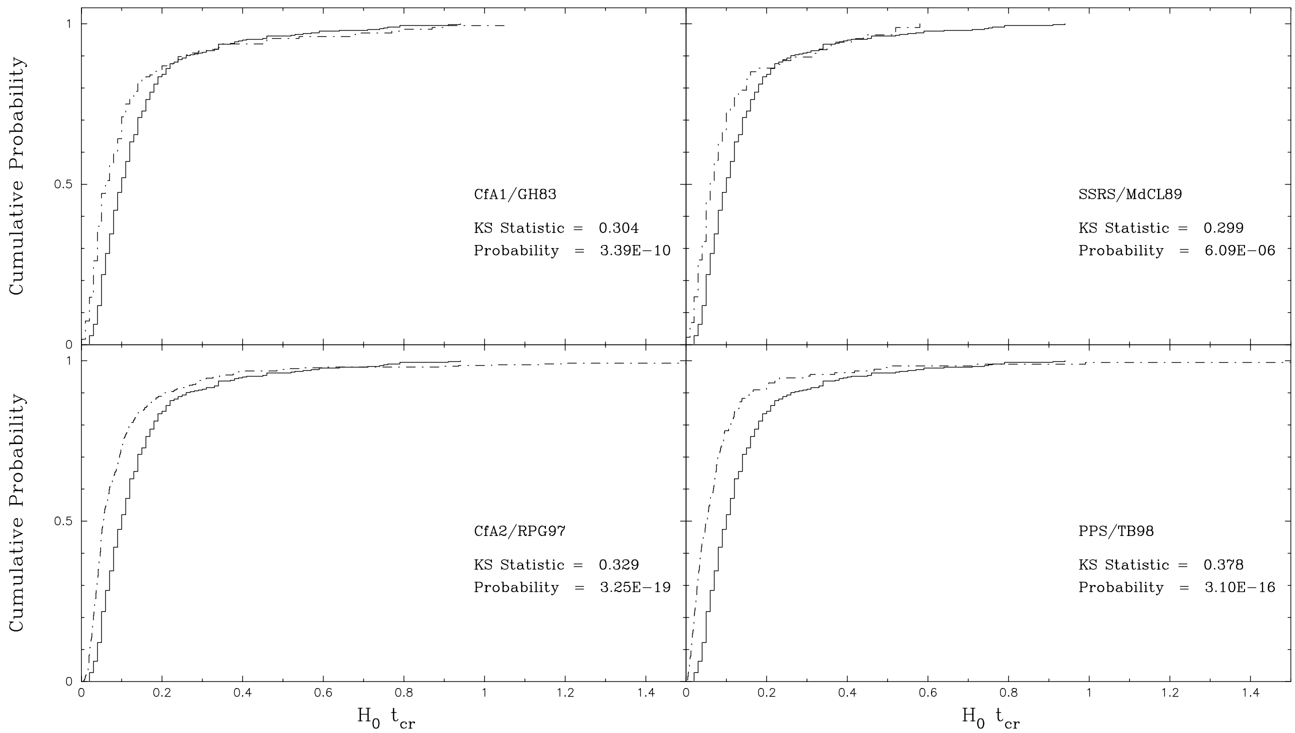

Fig. 24.— KS tests comparing the distribution of crossing times from various group catalogues (*dot-dashed line*) against that from the full LCRS group catalogue (*solid line*).

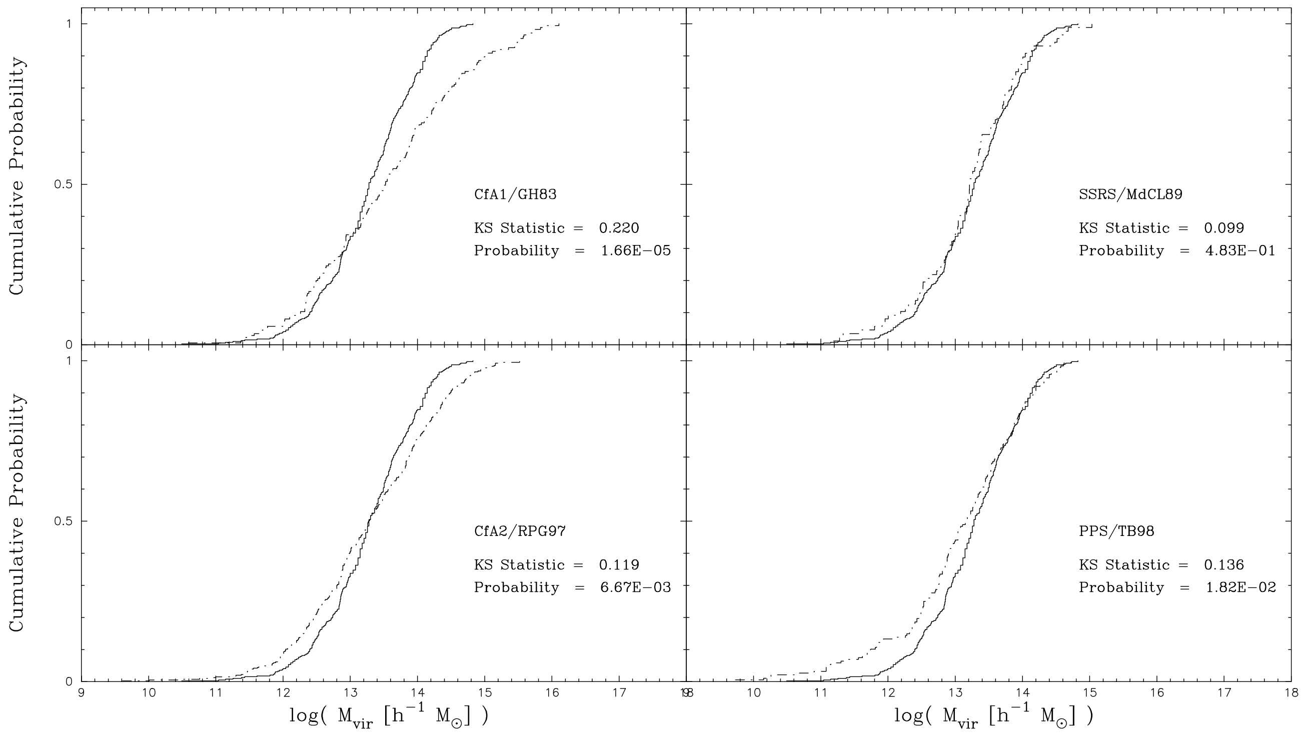

Fig. 25.— KS tests comparing the distribution of virial masses from various group catalogues (*dot-dashed line*) against that from the full LCRS group catalogue (*solid line*).

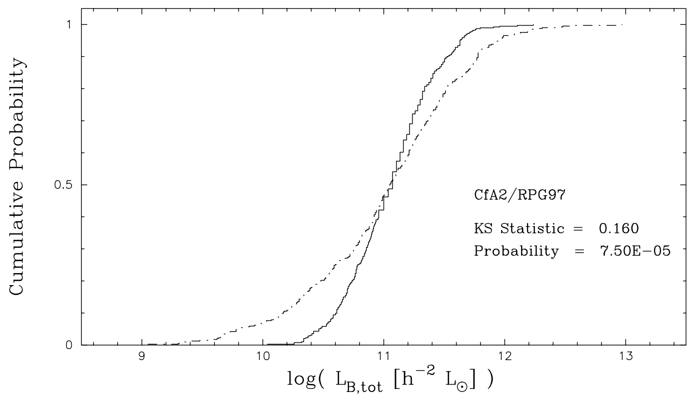

Fig. 26.— A KS tests comparing the distribution of de Vaucouleurs $B(0)$-band total group luminosities from RPG97 (*dot-dashed line*) against that from the full LCRS group catalogue (*solid line*). (The LCRS group luminosities have been converted from LCRS R-band to de Vaucouleurs $B(0)$-band via equation 39.)

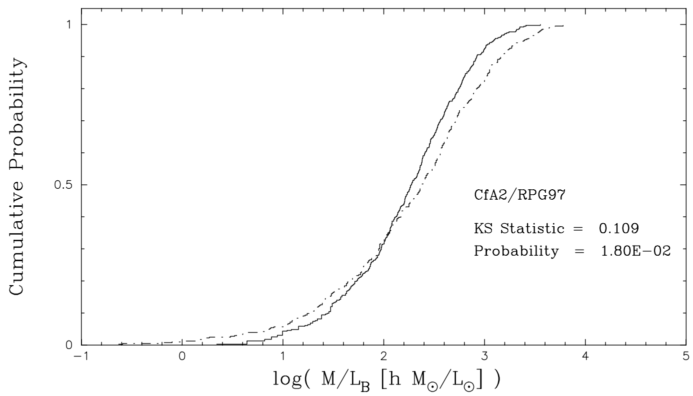

Fig. 27.— A KS tests comparing the distribution of de Vaucouleurs $B(0)$-band group mass-to-light ratios from RPG97 (*dot-dashed line*) against that from the full LCRS group catalogue (*solid line*). (The LCRS group luminosities have been converted from LCRS R-band to de Vaucouleurs $B(0)$-band via equation 39.)

TABLE 2

The Effects of the Value of the Edge Proximity Rejection Criterion on the Resulting Clean Sample

Distance from Slice Edge	$N_{\rm clean}$[a]	$\sigma_{\rm los}$ [km s^{-1}]		$R_{\rm p}$ [h^{-1} Mpc]		$R_{\rm h}$ [h^{-1} Mpc]	
		Mean	Median	Mean	Median	Mean	Median
$0 \times R_p$	739	155 ± 4	166	0.70 ± 0.01	0.750	0.65 ± 0.01	0.690
$1 \times R_p$	580	151 ± 4	164	0.67 ± 0.01	0.730	0.63 ± 0.01	0.640
$2 \times R_p$	394	152 ± 5	164	0.62 ± 0.02	0.640	0.58 ± 0.02	0.585
$3 \times R_p$	239	144 ± 6	155	0.51 ± 0.02	0.535	0.48 ± 0.02	0.475
$4 \times R_p$	136	144 ± 8	157	0.42 ± 0.02	0.430	0.40 ± 0.02	0.410

[a]The number of groups in the resulting clean sample.

TABLE 4

Comparison of Group Catalogues*

	LCRS					CfA1				SSRS	CfA2			PPS	ESP
	All	50	112	50/112	T94	GH83	NW87	N93	MFW93	MdCL89	RGH89 (all)	RGH89 (rich)†	RPG97	TB98	RZZ99
% of galaxies in groups	35%	30%	37%	…	23%	61%	61%	48%	55%	35%	44%	13%	42%	35%	40.5%
# of groups in catalogue	1495	274	1193	28	114	176	166	173	166	87	128	56	406	188	231
# of groups in clean sample	394	79	310	5	52	176	166	173	166	87	52	36	406	188	231
$<\sigma_{\rm los}>_{\rm med}$ [km s^{-1}]	164	211	150	286	177	223	123	116	155	183	209	228	192	194	194
$<H_0 t_{\rm cr}>_{\rm med}$	0.10	0.09	0.11	0.09	0.13	0.06	0.13	0.10	0.10	0.06	0.06	0.06	0.054	0.051	…
$<R_{\rm h}>_{\rm med}$ [h^{-1} Mpc]	0.58	0.75	0.55	0.71	0.75	0.55	0.67	0.48	…	0.48	0.51	0.52	0.43	0.34	…
$<R_{\rm p}>_{\rm med}$ [h^{-1} Mpc]	0.64	0.83	0.60	0.68	0.84	…	1.13	0.72	…	0.53	0.67	0.69	…	0.41	…
$<M_{\rm vir}>_{\rm med}$ [10^{13} h^{-1} $M_\odot$]	1.90	4.00	1.60	11.00	2.50	3.34	1.55	…	…	1.62	2.00	3.89	1.86	1.45	…
$<L_{\rm tot}>_{\rm med}$ [10^{11} h^{-2} $L_\odot$]‡	1.30	2.10	1.00	1.90	1.75	…	0.68	…	…	…	…	…	1.12	…	…
$<M/L>_{\rm med}$ [h $M_\odot/L_\odot$]‡	171	182	165	466	182	…	264	148	298	…	186	175	240	…	…

*Values for the non-LCRS group catalogues were taken from the original papers. Where necessary, values were converted to be consistent with the definitions associated with the LCRS group properties.

†RGH89 rich groups are those containing 5 or more members.

‡Luminosities for the LCRS group catalogues are in the LCRS R-band; for the various CfA1 and CfA2 group catalogues, in the de Vaucouleurs $B(0)$-band. A rough conversion is $L_R \sim 1.1 L_{B(0)}$ ($M/L_{B(0)} \sim 1.1 M/L_R$).

TABLE 5

THE SURVEY SAMPLES USED FOR THE DIFFERENT GROUP CATALOGUES

Group Catalogue	Survey	$N_{\rm gal}$[a]	$m_{\rm lim}$[b]	$z_{\rm med}$[c]	A[d] steradians
LCRS	LCRS	21,895	$16.0 \leq R < 17.3$ (50-fiber) $15.0 \leq R < 17.7$ (112-fiber)	0.075	0.21
GH83	CfA1	2,390	$m_{B(0)} = 14.5$	0.015	2.66
NW87	CfA1	2,345	$m_{B(0)} = 14.5$	0.015	2.66
N93	CfA1	2,398	$m_{B(0)} = 14.5$	0.015	2.66
MFW93	CfA1	≈2,400	$m_{B(0)} = 14.5$	0.015	2.66
MdCL89	SSRS	1,534	...[e]	0.020	1.75
RGH89	CfA2	1,766	$m_{B(0)} = 15.5$	0.025	0.42
RPG97	CfA2	6,062	$m_{B(0)} = 15.5$	0.025	1.2
TB98	PPS	3,014	$m_{B(0)} = 15.5$	0.025	0.76
RZZ99	ESP	3,342	$b_j = 19.4$	0.150	0.007

[a]The number of galaxies in the survey sample used to extract the group catalogue.

[b]The apparent magnitude limit(s) of the survey sample used to extract the group catalogue.

[c]The median redshift of the survey sample used to extract the group catalogue.

[d]The sky coverage of the survey sample used to extract the group catalogue.

[e]The SSRS is a diameter-limited, not a magnitude-limited, survey.

TABLE 6

KOLMOGOROV-SMIRNOV (KS) PROBABILITIES FOR SELECTED GROUP CATALOGUES

	GH83 log P	MdCL89 log P	RPG97 log P	TB98 log P	RZZ99 log P
$\sigma_{\rm los}$	-6.39	-0.66	-6.44	-2.33	-3.80
$H_0 t_{\rm cr}$	-9.47	-5.22	-18.49	-15.51	···
$R_{\rm h}$	-2.35	-2.53	-8.70	-13.88	···
$R_{\rm p}$	···	-2.56	···	-2.33	···
$M_{\rm vir}$	-4.78	-0.32	-2.18	-1.74	···
$L_{\rm tot}$	···	···	-4.12	···	···
M/L	···	···	-1.74	···	···

TABLE 7
LCRS Group – Abell Cluster Matches

N_{grp} (1)	α_{grp} (2)	δ_{grp} (3)	z_{grp} (4)	N_{obs} (5)	C_{grp} (6)	Abell (7)	α_{ACO} (8)	δ_{ACO} (9)	z_{ACO} (10)	R (11)	D (12)	C_{ACO} (13)	sep (′) (14)
LCRS −3° Slice													
72†	11 09 59.52	-02 54 39.8	0.0825	14	24 ± 6.4	1200	11 09.8	-02 53	···	1	5	53	3.32
73†	11 10 02.26	-02 57 05.7	0.0883	9	20 ± 6.7	1200	11 09.8	-02 53	···	1	5	53	5.43
126†	11 48 25.10	-02 52 27.1	0.1302	9	59 ± 19.7	1399	11 48.6	-02 49	0.0913[a]	2	4	82	4.40
173†	12 58 21.16	-03 10 17.3	0.0725	3	16 ± 9.2	1658	12 58.6	-03 10	···	1	5	50	3.72
184†	13 21 31.01	-03 11 19.4	0.0849	4	16 ± 8.0	1729	13 21.4	-03 06	···	1	5	76	5.60
279†	15 11 42.71	-02 34 14.5	0.1045	6	19 ± 7.8	2045	15 11.6	-02 34	···	1	5	53	1.69
LCRS −6° Slice													
147	15 09 55.99	-05 43 47.3	0.1170	6	36 ± 14.7	2035	15 09.5	-05 52	···	1	5	57	10.45
LCRS −12° Slice													
94†	11 38 38.74	-12 05 01.0	0.1183	5	24 ± 10.7	1348	11 38.7	-12 05	0.1195[b]	2	5	99	0.80
145†	12 42 07.88	-11 49 35.6	0.1382	7	47 ± 17.8	1606	12 42.0	-11 43	···	1	5	51	6.87
276	15 19 37.20	-11 55 56.4	0.1495	4	24 ± 12.0	2060	15 19.6	-11 59	···	1	6	65	3.07
LCRS −39° Slice													
17	00 36 17.54	-39 06 00.4	0.1009	4	10 ± 5.0	S64	00 36.7	-39 08	···	···	5	10	5.15
20†	00 41 20.76	-39 29 56.8	0.1080	3	10 ± 5.8	S73	00 41.8	-39 38	···	···	5	21	9.61
24†	00 45 45.21	-38 44 30.8	0.1340	3	15 ± 8.7	2822	00 45.9	-38 44	···	1	6	67	1.79
32†	01 03 01.86	-38 48 00.7	0.0771	3	12 ± 6.9	S123	01 03.4	-38 41	···	···	6	27	8.23
72	02 28 38.24	-38 51 50.7	0.1256	3	18 ± 10.4	3029	02 28.9	-38 55	···	1	6	72	4.40
98	03 16 23.99	-39 16 08.3	0.1333	3	19 ± 11.0	3114	03 16.4	-39 18	···	0	6	45	1.86
138†	04 04 09.84	-38 58 45.9	0.0561	14	14 ± 3.7	S418	04 04.2	-39 00	0.042[c]	···	3	12	1.30
139	04 04 40.06	-38 50 29.6	0.0517	3	3 ± 1.7	S418	04 04.2	-39 00	0.042[c]	···	3	12	10.96
145†	04 16 17.59	-39 08 33.6	0.0502	4	4 ± 2.0	3239	04 15.7	-39 04	···	2	6	81	8.27
171†	21 26 18.86	-38 45 51.7	0.1328	3	20 ± 11.5	S948	21 26.9	-38 39	···	0	6	40	9.70
172†	21 26 31.51	-38 50 06.9	0.0763	7	13 ± 4.9	S948	21 26.9	-38 39	···	0	6	40	11.95
185†	22 03 03.62	-38 20 38.4	0.1107	3	11 ± 6.4	S992	22 02.7	-38 23	···	···	6	27	4.85
186†	22 03 38.91	-39 27 22.9	0.0696	7	10 ± 3.8	S993	22 03.7	-39 29	···	···	5	19	1.72
191†	22 15 20.58	-39 04 32.9	0.1407	19	91 ± 23.5	3856	22 15.8	-39 09	0.1260[d]	2	5	125	6.94
195†	22 19 17.65	-38 54 45.2	0.0719	4	8 ± 4.0	S1016	22 19.3	-38 55	···	···	5	-10	0.26
200	22 33 23.71	-39 02 26.0	0.1486	5	80 ± 35.8	S1042	22 32.9	-38 59	···	···	5	5	6.72
202	22 36 35.59	-38 53 47.5	0.0645	3	4 ± 2.3	3899	22 37.4	-38 51	···	0	5	37	9.83
231	23 22 20.99	-38 55 52.4	0.1298	3	16 ± 9.2	S1120	23 22.0	-38 57	···	···	6	6	4.23
244	23 41 13.50	-38 32 14.3	0.1004	3	12 ± 6.9	4029	23 41.0	-38 33	···	0	5	43	2.75
256†	23 59 16.96	-39 09 47.3	0.1022	3	10 ± 5.8	S1172	23 58.8	-39 03	0.0500[a]	···	4	8	8.81
LCRS −42° Slice													
3†	00 01 43.09	-42 12 55.7	0.1246	6	39 ± 15.9	2718	00 01.1	-42 13	···	1	5	61	6.87
10†	00 16 08.74	-42 07 58.9	0.0931	17	39 ± 9.5	2758	00 15.9	-42 03	0.092[e]	0	5	37	5.68
12	00 18 00.87	-42 06 18.8	0.0529	4	5 ± 2.5	2763	00 17.5	-42 14	···	1	6	58	9.58
39	01 03 11.93	-41 55 13.7	0.0980	5	10 ± 4.5	S122	01 03.3	-41 56	···	···	5	-35	1.37
52†	01 39 05.34	-42 27 51.1	0.0960	5	12 ± 5.4	S180	01 39.9	-42 22	0.0500[c]	···	5	20	10.72
65	02 01 24.48	-41 21 01.3	0.1235	5	21 ± 9.4	2969	02 01.5	-41 20	0.12397[f]	2	5	83	1.46
66†	02 01 36.36	-41 22 49.1	0.1295	7	41 ± 15.5	2969	02 01.5	-41 20	0.12397[f]	2	5	83	3.06
78†	02 32 39.79	-41 43 33.9	0.0703	11	14 ± 4.2	S281	02 33.2	-41 47	···	···	5	11	6.92
79†	02 33 27.21	-41 50 19.2	0.1072	12	34 ± 9.8	S281	02 33.2	-41 47	···	···	5	11	4.37
80	02 34 16.48	-42 04 26.8	0.0972	3	9 ± 5.2	3033	02 34.2	-41 59	···	0	6	31	5.51
86	02 45 53.05	-41 57 40.5	0.0704	7	29 ± 11.0	S297	02 45.6	-42 02	0.07092[f]	···	4	6	5.36
131†	04 17 08.84	-42 15 47.2	0.0545	10	10 ± 3.2	S436	04 17.1	-42 19	···	···	5	0	3.26
223	23 00 49.64	-42 34 39.9	0.1357	3	22 ± 12.7	S1084	23 00.8	-42 37	···	···	5	20	2.35
234†	23 16 36.79	-42 13 36.1	0.1132	8	46 ± 16.3	S1111	23 16.4	-42 22	0.045[g]	···	4	25	8.73
LCRS −45° Slice													
75	02 05 32.60	-45 02 20.5	0.1047	9	27 ± 9.0	S224	02 05.0	-45 09	···	···	6	26	8.80
87†	02 21 40.61	-44 53 28.3	0.0945	5	12 ± 5.4	S253	02 21.7	-44 53	···	···	5	1	0.53
88	02 22 34.96	-44 58 29.3	0.0646	7	13 ± 4.9	S253	02 21.7	-44 53	···	···	5	1	10.86
91	02 35 19.03	-45 08 34.1	0.1464	4	42 ± 21.0	S286	02 34.7	-45 04	···	···	6	25	7.97
92†	02 35 27.41	-45 12 16.4	0.0651	3	6 ± 3.5	S286	02 34.7	-45 04	···	···	6	25	11.51
97	02 42 54.87	-45 22 55.7	0.0969	4	10 ± 5.0	S293	02 43.1	-45 26	···	···	6	-16	3.64
115†	03 34 08.23	-45 17 24.1	0.0676	10	13 ± 4.1	S367	03 33.8	-45 20	0.0666[a]	···	4	-13	4.40
179†	21 38 42.89	-44 36 54.3	0.0985	6	15 ± 6.1	3800	21 38.5	-44 35	···	0	6	48	2.98
232†	22 58 10.82	-45 26 22.2	0.0992	5	15 ± 6.7	3953	22 57.4	-45 35	···	0	6	39	11.91
236†	23 00 45.32	-44 40 39.9	0.0682	13	20 ± 5.5	3963	23 01.0	-44 35	0.0890[a]	0	5	40	6.24

† Includes as a member at least one 55 arcsec "orphan" with a faked velocity.
[a] Abell, Corwin, & Olowin (1989).
[b] Ebeling et al. 1996; obtained from the NASA/IPAC Extragalactic Database (NED).
[c] Olowin, De Souza, & Chincarini 1988; obtained from the NASA/IPAC Extragalactic Database (NED).
[d] Ebeling & Maddox 1995; obtained from the NASA/IPAC Extragalactic Database (NED).
[e] Dalton et al. 1994; obtained from the NASA/IPAC Extragalactic Database (NED).
[f] Collins et al. 1995; obtained from the NASA/IPAC Extragalactic Database (NED).
[g] Stocke et al. 1991; obtained from the NASA/IPAC Extragalactic Database (NED).